AEROJET-GENERAL CORPORATION
Research and Engineering Division
11711 Woodruff Avenue
Downey, California

BLAST AND FIREBALL COMPARISON OF CRYOGENIC AND HYPERGOLIC PROPELLANTS WITH SIMULATED TANKAGE

Addendum to Report 0822-01(01)FP

Contract No. NAS 9-2055

0822-01(02)FP

Prepared for

Gemini Program Office
National Aeronautics and Space Administration
Manned Spacecraft Center
Houston, Texas

Prepared by: R. E. Pesante
R. D. Erickson
D. G. Frutchey
W. J. Helm

Date: June 1964

No. of Pages: 62

Classification: UNCLASSIFIED

Reviewed by: D V Paulson
D. V. Paulson, Head
Propellant Physics Department
Research Division

Approved by: H J Fisher
H. J. Fisher, Manager
Research Division

CONTENTS

TABLES

FIGURES

FIGURES (cont)

1. INTRODUCTION

A comparison of the basic blast properties of hypergolic and cryogenic propellants was obtained in the basic study (Reference 1) under carefully controlled test conditions of contact area and oxidizer/fuel ratios. No attempt was made during the basic study to simulate actual missile configurations. The purpose of the study reported here was to obtain accurate estimates of the hazards to personnel and equipment resulting from nitrogen tetroxide (N_2O_4) and a 50/50 mixture of hydrazine and unsymmetrical dimethyl hydrazine (UDMH) propellant in simulated missile tankage containing 300 lb of propellant.

It was not the intent of this program to obtain data for the purpose of extrapolating to larger quantities of propellant, nor was it intended for the experimental data to be construed as the complete answer to the full-scale evaluation of the explosive characteristics of a launch vehicle booster containing either hypergolic or cryogenic propellants.

2. OBJECTIVE

The objective of this program was to compare the blast and radiant properties of hypergolic propellants with cryogenic propellant under simulated space booster launch conditions involving tankage failure modes caused by accelerations in a fall-back situation (hereafter referred to as the fall-back failure mode) and by the decelerations in a sudden loss of thrust only (hereafter referred to as the static failure mode).

Specific parameters to be considered in establishing a comparison between the two propellant types were peak overpressure, shockwave velocity, positive impulse and duration, and radiant heat flux as well as fireball temperature, duration, and size.

All test measurements were to be obtained with instrumentation developed in Reference 1.

3. SUMMARY

A total of eight tests were conducted from 15 April to 19 May 1964, to permit a basic comparison of the explosive and fireball characteristics of hypergolic and cryogenic propellants. The propellants were combined with simulated missile booster tankage in deceleration and acceleration failure modes for a 300 lb total quantity of material.

Mixing of the propellants was accomplished by rupturing a glass or aluminum diaphragm between the fuel and oxidizer sections of a thin-wall aluminum tank. Measurements of peak overpressure, positive impulse, temperature, and heat flux were made at distances of 10, 25, and 40 feet from the test article in each of the four surrounding quadrants. Thermal radiation data and motion picture coverage were also obtained from each test.

16 12 71 2

Analysis of the test results indicated that the cryogenic propellant tests yielded TNT equivalences of 0.01 to 0.15 lb of TNT per lb of propellant on a peak overpressure basis and approximately 0.01 to 0.20 lb of TNT per lb propellant on an impulse basis. The hypergolic propellant tests indicated TNT equivalences of less than 0.01 lb of TNT per lb of propellant for all tests in both failure modes.

The two cryogenic fallback failure mode tests initiated spontaneously approximately 0.05 sec after impact from a drop height of 15 ft. No explanation was readily available for this phenomena of initiation.

The fireballs produced by the propellants were related in some respects to the failure mode. The fallback failure mode tests with both cryogenic and hypergolic propellants yielded fireball heights that did not exceed 38 ft. The cryogenic test diameters extended to 117 ft compared to 58 ft for the hypergolic tests. The static failure mode tests with cryogenic propellants, yielded diameters of 65 to 85 ft and heights of 90 and 95 ft. The static failure mode hypergolic tests indicated heights up to 82 ft and diameters up to 53 ft.

Maximum fireball temperatures of 2828°F and 3039°F were observed for the LOX/RP-1 and N_2O_4/A-50 propellants, respectively. Total thermal radiation yields from 7.3×10^6 to 2.3×10^9 joules were observed for the LOX/RP-1 tests. The hypergolic tests indicated

yields which ranged from 6.7×10^7 to 1.19×10^8 joules. Results of the thermal radiation and temperature measurements were used to calculate emissivity values for the fireballs. These measurements indicated emissivity values of 0.45 to 0.55 for the cryogenic tests and approximately 0.25 for the hypergolic tests.

Author

4. TECHNICAL DISCUSSION

4.1 APPROACH

Although several test programs to determine the explosion and thermal radiation hazards of hypergolic propellants have been conducted with simulated tankage by various agencies (References 2 through 6), none have measured completely: (1) the thermal energy emitted; (2) the blast effect; or (3) the fall-back failure mode. The objectives of this program were approached with the concept of eliminating test variables, such as contact area and oxidizer/fuel ratio, that had been experienced in previous tests with simulated tankage.

4.2 TEST FIXTURE DESIGN

The test fixture consisted of a cylindrical aluminum tank which was divided into two sections to contain the oxidizer and the fuel. A typical static failure mode tank is shown in Figure 1. Separation of the propellants during test preparations was accomplished by either a tempered glass (0.25 in. thickness) or aluminum diaphragm (0.003 in. thickness) which was positioned between the two tank sections. Oxidizer/fuel mixing was accomplished by rapid removal of the diaphragm with the tankage in a vertical position. Removal of the diaphragm was accomplished with two techniques to satisfy the test objectives of a static and fall-back failure mode. Removal of the aluminum diaphragm for the static failure mode was accomplished by cutting the diaphragm with a shockwave from a length of mild detonating cord. The glass diaphragm for the fall-back failure mode was removed by a pointed metal ram and wiper ring which pierced the glass on impact.

The tankage dimensions were determined by the weight of propellant, mixture ratios, and tankage length-to-diameter ratios. The total weight of the propellant sample in each test was limited to 300 lb to permit direct comparison with data from previous studies (Reference 1). The mixture ratios were selected at oxidizer/fuel ratios of 2:1 for the hypergolic and 2.5:1 for the cryogenic. A tankage length-to-diameter ratio of 1.8:1 was chosen for the cryogenic propellant and 1.6:1 for the hypergolic propellant. These length-to-diameter ratios necessitated a tank diameter of 17.75 in. or 247 $in.^2$ of contact-area for the specified weight of propellants. A propellant test plan was devised that evaluated the two failure modes for each propellant in duplicate, or a total of four tests for each type of propellant. The test plan is presented in Table 1.

The propellant tanks were fabricated from sheet aluminum. The cylindrical tank wall was 0.10-in.-thick sheet welded to 0.10-in.-thick ends. The two tank sections were welded to two 0.5-in.-thick aluminum flanges which were designed to permit insertion of the rupture diaphragms. The two flanges were joined with twelve 0.5 in. bolts with a thin polyethylene gasket on each side of the rupture diaphragm.

The lower tank section was designed to provide an 18 in. separation between the rupture diaphragm and the surface of the propellant. This separation between the oxidizer and the fuel surfaces provided a propellant impact velocity (computed) of approximately 9.8 ft/sec for the static test mode.

4.3 TEST OPERATIONS

The two failure modes necessitated development of the two test assembly procedures described in the following sections.

4.3.1 Static Failure Mode

The lower tankage section was placed on a steel plate in the center of the test area (Figure 2) and loaded with the quantity of oxidizer required. The cryogenic test required insulation around the lower tank section to prevent rapid vaporization of the LOX (Figure 3). The aluminum rupture diaphragm was placed over the lower section flange. A small vent was fabricated in the side of the lower tank section to prevent pressure

build-up in the tank which might rupture the thin aluminum disk during test preparations. A length of plastic tubing was attached to this vent for the hypergolic test to permit exhaust of the oxidizer vapor away from the fuel tank section and eliminate any possible ignition of the propellants before the programed time.

The cryogenic test tankage was fitted with a small charge of explosive to initiate the propellants after mixing. A No. 8 blasting cap and 8.5-gram tetryl pellet were located above the level of the oxidizer in a plastic bag secured to a rigid support to prevent relocation of the initiator during the mixing period.

The lead-covered mild-detonating cord necessary to rupture the aluminum diaphragm was placed in a circular position on top of the aluminum discs approximately 1 in. from the tank wall (Figure 4). Flexible plastic tubing was placed over the detonating cord and plugged at one end with a stopper to contain the lead fragments and prevent initiation of the fuel. The plastic tubing permitted transfer of the shockwave in sufficient intensity to rupture the aluminum diaphragm without rupture of the tubing wall or damage to the tank walls. The detonating cord was positioned to leave intact a small section of the diaphragm to serve as a hinge and prevent the cut-out section of the diaphragm from dropping into the mixing reaction between the oxidizer and the fuel. The end of the detonating cord was passed out the side of the upper tank above the liquid level and connected to a No. 8 blasting cap.

To provide for personnel safety, the fuel was added (at a rate of $\approx$1 gal/min) to the upper tankage section by remote control. The loading operation was accomplished from a reinforced concrete instrumentation and personnel building.

An air-driven fuel pump and a reservoir were located in a pit adjacent to the test fixture. Prior to each test, a small quantity of fuel was placed in the fuel reservoir tank, and the tank was then pumped dry to fill the pump and transfer lines. The desired quantity of test fuel, which had been carefully measured previously in a separate vessel, was then added to the fuel reservoir adjacent to the fuel pump. The tank was pumped dry (remotely) to obtain the desired amount of fuel

in the upper tank section. Transfer of the fuel was accomplished through a flexible line connected to the upper tank above the final expected liquid level to prevent siphoning of the fuel back into the reservoir.

At a predetermined time, the detonating cord was initiated and the various blast and thermal radiation parameters were measured. The initiation charges for the two cryogenic tests were programed to fire with delays of 0.1 and 0.4 second after contact of the oxidizer and fuel.

4.3.2 Fall-Back Failure Mode

The fall-back failure mode tankage tests were accomplished with techniques similar to those used in the static tests except that the position of the fuel and oxidizer was reversed in the tankage; i.e., the oxidizer was located in the upper section and fuel was located in the lower section. A structural member was added to the sides and top of the upper tank section to permit connection of the lifting mechanism to the assembled tank. The empty tank was assembled with a tempered glass diaphragm (20 in. dia by 0.25 in. thickness) between the two tank sections and a weighted ram in the upper tank section (Figures 5 and 6). The tempered glass was employed as a diaphragm material to utilize its physical property of breaking into small pieces when shock loaded. Fracture of the glass into small pieces permitted a uniform cross-sectional contact area between the oxidizer and fuel during mixing.

The oxidizer was loaded into the upper tank section through a hole in the top of the tank. Provision for addition of the fuel to the tankage was made by placing a plastic line between the lower tank section and the fuel pump.

A small explosive charge was used in the two cryogenic fall-back tests to initiate the propellants at a predetermined time after impact. The charge consisted of a No. 8 blasting cap and 8.5-gram tetryl pellet which were located above the expected fuel level in the lower tank section. The explosive charge was secured to a rigid support to prevent relocation during the mixing period.

The assembly tankage and oxidizer were raised to an impact height of 15 ft on a 22-ft-high drop tower with a hand-operated winch. To provide stability to the tankage during raising operations and ensure its proper attitude during the subsequent fall, guide cables were secured with eyebolt or tubing guides at four positions around the circumference of the both the upper and lower tank sections. The fuel was added by remote control to the tankage in the elevated position with a technique duplicating the fuel-loading operation for the static tankage. The tankage assembly was released at the desired time by an exploding-bolt release mechanism. The drop tower, test area, and a fall-back failure mode tank are shown in Figure 7. A cryogenic tank in the elevated drop position is shown in Figure 8.

Propellant mixing was accomplished by driving the ram through the tempered glass on impact. The ram consisted of a lead-filled 26-inch length of 1-in. diameter steel pipe with a pointed steel rod secured in the end. Approximately 2 in. above the point, a metal ring 15 in. in diameter was welded to the ram to serve as a wiper to remove any pieces of glass which might have remained after the initial breakthrough of the ram point.

4.4 DIAPHRAGM RUPTURE TESTS

A series of preliminary shatter tests was conducted to determine the efficiency of the diaphragm rupture techniques. A test with a length of mild detonating fuze (MDF) arranged in a cross pattern and water replacing the fuel in the upper tank failed to remove the desired amount of diaphragm material. For the next test, the MDF charge was moved to the top of the diaphragm and the pattern changed to a circular layout. This configuration proved successful and approximately 90% of the diaphragm area was removed. Some doubt as to the advisability of initiating the lead-covered MDF in the fuel led to the enclosing of the cord in the plastic tubing to prevent any source of initiation for the fuel.

A single preliminary drop test was conducted with the fall-back failure mode tankage. The diaphragm was completely removed by the ram and wiper action with a water-filled upper tank. Examination of the test remains indicated the glass had fragmented in approximately 0.25-in. size pieces.

4.5 FALL-BACK FAILURE-MODE TANKAGE IMPACT VELOCITY

The impact velocity of the fall-back failure mode tankage was determined with a high-speed camera and grid system. A Fastax camera (2000 fps) was positioned to record the fall of the tankage in reference to a position grid (Figure 5). The camera records were used to determine the time history of the tank and to calculate the impact velocity.

4.6 TEST RESULTS

The test results from the experimental studies conducted on this program are presented in Tables 2 through 8.

4.6.1 Air Blast Equivalence

The overpressure measurements for the two failure modes are presented in Figures 9 and 10 with the pertinent TNT equivalence calibration curves (References 1, 7, and 8). The impulse calibration data are presented in Figures 11 and 12 by superimposing the pertinent TNT equivalence curves over the results of the impulse measurements for the two failure mode conditions. The calibration curves permit a direct evaluation of the TNT equivalence for each test condition on both an impulse and pressure basis.

The TNT equivalence comparison must be made with caution and with a simultaneous evaluation of peak overpressure and positive impulse data. The initial air shock produced from an explosive material is increased, by the support it receives from expanding gases and secondary shocks, to a point where it assumes the characteristics of a shockwave produced from a point source. This unsupported shock-wave does not form until the shockwave has traveled beyond the fire-ball limits.

Comparison of the peak overpressure and impulse test results indicated a substantial difference in the blast yields from the two propellants for both the static and fall-back failure modes. The peak overpressure and impulse data for the hypergolic propellant tests indicated TNT equivalences of less than 0.01 lb of TNT per lb of propellant for both failure modes. The two cryogenic tests with static tankage yielded

TNT peak overpressure equivalences (Figure 9) that varied from 0.05 to 0.07 lb of TNT per lb of propellant for a 0.4 sec initiation delay after the initiation of mixing and approximately 0.01 lb of TNT per lb of propellant for a 0.1 sec initiation delay after initiation of mixing. The two cryogenic fall-back tests yielded TNT peak overpressure equivalences (Figure 10) from 0.05 to 0.18 lb of TNT per lb of propellant. Examination of the cryogenic impulse data for the static failure mode indicated TNT equivalences (Figure 11) that varied from less than 0.01 lb of TNT per lb of propellant for the 0.1 sec mixing delay to between 0.8 and 0.15 lb of TNT per lb of propellant for a 0.4 sec mixing delay before initiation. The cryogenic fall-back failure mode impulse results indicated equivalences (Figure 12) that varied from 0.20 to 0.14 lb of TNT per lb of propellant.

Analysis of the cryogenic static failure mode tests indicates the mixing period before initiation has a substantial effect on both the peak pressure and impulse yields. Although only two delay tests were conducted, it is evident that a cryogenic sample with a 0.4 sec delay period can produce blast yields 7 to 5 times greater in magnitude than a cryogenic sample with a 0.1 sec delay. The longer delay time is believed to permit more extensive mixing of the oxidizer and fuel, thus enhancing a higher rate and greater amount of energy release.

Comparison of the cryogenic test results for the two failure modes indicated the fall-back failure mode peak overpressure and impulse equivalences are two to three times greater in magnitude than the peak overpressure and impulse equivalence for the static failure mode. This increase in yield is attributed to greater quantity of mixed propellant in the fall-back failure mode due to the impact momentum of the propellant.

Although the peak overpressure yields of the hypergolic fall-back tests were higher than the static failure mode test yields, the magnitude of the differences (0.15 to 1.2 psi) was substantially lower than the pressures from the cryogenic propellants. The higher yields are again attributed to the greater quantities of propellant which are forced together in the fall-back failure mode due to the impact momentum of the propellants.

4.6.2 Cryogenic Propellant Initiation

The test plan for the cryogenic tests included provisions for an initiation delay at a predetermined time after the initial contact of the oxidizer and fuel. The delay period was intended to permit ultimate participation of the fuel and oxidizer in the explosive reaction. However, the fall-back failure mode tests initiated spontaneously approximately 0.05 sec after impact of the aluminum tank on the steel plate. The cause of the initiation is unknown, but possible causes are the compression of the LOX/RP-1 propellant between the glass diaphragm fragments and the tank wall or bottom or a pressure and combustion buildup inside the tank which shifted into a detonation reaction.

4.6.3 Shock Pulse Characteristics

Examination of the pressure-pulse records indicates that the pressure-time characteristics of the blast waves were similar to those of conventional explosives for all cryogenic tests and for the fall-back failure mode hypergolic tests. The static failure mode hypergolic tests yielded readable pressure records in only one of the two tests conducted. The first static hypergolic test yielded overpressures of less than 0.25 psi, which was below the instrumentation sensitivity level. The hypergolic test which produced a readable record yielded three separate pulses with a gradual pressure rise at the leading edge instead of the characteristic sharp pressure rise observed in other tests. The rise rate was dependent on the distance of the pressure transducer from the propellant sample. In all hypergolic tests which produced a reducible test record, the shockwave velocity was near the sound velocity for the atmospheric conditions experienced. The cryogenic shockwave velocities were above 1400 ft/sec except for the 0.1 sec mix delay test. In this test the velocities were near 1200 ft/sec.

4.6.4 Fireball History

The results of the fireball size and duration measurements are illustrated in Figures 13 and 14 and listed in Table 4. The fireballs produced by the cryogenic propellants were related to the failure mode. The static failure mode tests yielded fireballs of symmetrical

dimensions with maximum height which ranged from 90 to 95 ft and diameters which ranged from 67 to 85 ft. The fall-back failure mode tests produced fireballs with large diameters and small heights. This fireball shape was caused by the impact of the propellant against the steel plate causing the propellant fireball to expand close to the ground. The fireballs had diameter-to-height ratios of approximately 3 to 1 for both tests. Heights of 35 to 38 ft and diameters of 113 and 117 ft were observed.

The hypergolic tests yielded fireballs which depended on the tankage failure mode (Figure 14). The first static failure mode hypergolic test resulted in the bottom of the tankage being blown off and the rest of the tankage launched in the air as a missile in a vertical flight. The fireball from this test reached 81 ft in height and 53 ft in diameter. It is significant that the propellant reaction was not of sufficient magnitude to cause further damage to the tankage. The second hypergolic test resulted in the top of the tankage being blown off, and was followed by three separate fireballs. The camera coverage was not of sufficient length to cover the entire duration of the third fireball.

A maximum height of 23 ft and maximum diameter of 30 ft were observed during this test. A still photograph made from movie camera coverage of the fireball is shown in Figure 15. The fireball in this test was nearly transparent during most of its duration.

The fall-back failure mode hypergolic tests produced fireballs with relatively small dimensions. The tests indicated heights of 32 and 35 ft and diameters of 51 and 55 ft (Figures 16 and 17). An enlargement of a high-speed (600 frames/sec) camera frame of one of these tests is shown in Figure 18. Notice the dark cloud of N_2O_4 fumes which were projected upward from the fireball. Most of this cloud failed to enter into the combustion reaction and dispersed in the atmosphere after the fireball terminated.

Comparison of the fireball durations for the two propellants indicated a definite relationship only in the fall-back failure mode tests. The durations of the LOX/RP-1 fireballs were shorter than the N_2O_4/A-50 fireballs. The LOX/RP-1 propellant combinations yielded fireballs of 2.0 and 2.45 sec duration, while the N_2O_4/A-50 tests yielded fireball durations of approximately 3.7 and 4.2 sec (Figures 16 and 17).

The static failure mode tests did not indicate a definite trend regarding fireball duration, although it is significant that both cryogenic tests terminated at approximately the same time (3.2 sec) after impact even with a considerable difference in the mixing delay period. The hypergolic static failure mode tests produced fireballs with durations of approximately 2.7 sec for the tankage that failed at the bottom and 5.5 sec for the tankage that failed at the top.

4.6.5 Radiation Tests

The results of the thermal radiation measurements are presented in Tables 5 and 6 and shown in Figures 19 and 20 in the form of apparent effective fireball radiant intensity vs time for each of the five spectral regions. The units of intensity are given in watts per steradian; that is, power emitted per unit solid angle. These values may be converted to irradiance (incident power per unit area) by dividing by the range squared.

The integrated total yield is reported for each test in Table 4. These values were calculated by numerical integration of the total intensity vs time, assuming spherical symmetry for the radiation; i.e., the integral was multiplied by 4π.

Examination of the total yield data did not indicate a definite trend or relationship in the fireball total radiation. The results of the static failure mode cryogenic tests are slightly higher than those of the hypergolic static failure mode tests. The cryogenic tests indicated total yields of 3.0 and 3.4×10^8 joules compared to the hypergolic total yields of 1.19×10^8 and 9.30×10^7 joules.

The fall-back failure mode tests indicated yields which varied considerably. For the cryogenic tests, total yields of 2.3×10^9 and 7.3×10^6 joules were observed. The hypergolic tests indicated yields of 9.6 and 6.7×10^7 joules for the same failure mode. The wide difference in the two cryogenic tests is not readily explanable by the test results, but is probably connected with the mixing period before initiation of the propellant.

In previous studies (Reference 1) a partitioning of blast energy was observed for the propellant tests; i.e., the higher the peak overpressure and impulse produced in a given test, the lower the thermal radiation yield. The results of this program did not indicate a definite partitioning of energy as in the previous study, although the data indicate a slight trend in this direction. One of the fall-back failure mode cryogenic tests produced a higher thermal radiation and peak overpressures yield than either of the two hypergolic static failure mode tests, which indicate low pressure values.

The radiation data of the hypergolic and cryogenic propellant tests did indicate a relationship between time-to-maximum-intensity after initiation of the propellant and other test parameters. All of the cryogenic tests, both static and fall-back failure modes, had shorter time-to-maximum-intensities than the hypergolic tests. The cryogenic test peak intensities occurred approximately 0.15 to 0.6 sec after initiation for the two static tests and 0.2 to 1.3 sec after initiation for the two fall-back tests. The hypergolic tests indicated peak intensities which occurred from approximately 1.35 to 1.90 sec after initiation.

The results of the heat flux gage measurements are reported in Table 3 in terms of the maximum recorded energy observed at each gage station. Examination of the gage results indicates a wide variation in recorded values depending on the position of the gage in reference to the fireball growth and wind drift. Results of the N_2O_4 tests indicated maximum flux values which varied from 36.7 to 1.4 BTU/ft-sec for the fall-back failure mode and from 26.5 to 0.7 BTU/ft-sec for the static failure mode. The static failure mode hypergolic test that burned for several seconds yielded heat flux values which were approximately 50% or less of the other hypergolic test values.

The cryogenic test results yielded maximum heat flux values of 129.2 to 12.2 BTU/ft-sec for the fall-back failure mode studies and from 89.3 to 5.0 BTU/ft-sec for the static failure mode studies. It is readily evident that the cryogenic tests produced higher maximum values in all tests.

The duration from rupture of the diaphragm material until maximum flux value varied with the type of propellant and failure mode. A typical cryogenic and hypergolic heat flux record is shown in Figures 21 and 22 for the static failure mode. The data are shown in terms of the heat flux vs time from diaphragm rupture for both failure modes. These two curves indicate the hypergolic tests had shorter durations for the static failure mode, although the maximum values were lower. The cryogenic peak flux values occurred from 0.65 to 0.9 sec after diaphragm rupture, while the hypergolic peak flux values occurred from 0.3 to 0.4 sec after rupture. The fall-back failure mode indicated a reverse in this order in that the cryogenic peak flux values occurred approximately 0.2 seconds after rupture (Figure 23) and the hypergolic test peak flux values occurred from 1.0 to 2.0 seconds after rupture. The long duration times for the hypergolic tests are attributed to the size and growth rate of the fireballs. The hypergolic tests produced flat small diameter fireballs when compared to the cryogenic tests. The initial growth rate of the cryogenic fireballs exceeded that of the hypergolic fireballs by approximately 100 percent.

4.6.6 Fireball Temperature

The maximum temperature measurements are reported in Table 3 as the maximum observed value in degrees Fahrenheit at each gage station. Examination of the temperature data indicates a variation in the recorded values depending on the position of the thermocouples in reference to the fireball shape and wind drift. No definite relationship was observed between maximum temperature and other test parameters except that the static failure mode hypergolic test yielded appreciably lower temperatures than other tests. This is attributed to the small fireball diameter observed for the test. The maximum temperature observed for the hypergolic tests was 3039°F in the fall-back failure mode and 2828°F for the cryogenic fall-back failure mode.

Typical hypergolic and cryogenic temperature records are presented in Figures 24 and 25 for the fall-back failure mode tankage. The temperatures are plotted in terms of the time duration from rupture of the diaphragm between the oxidizer and fuel. The time to maximum temperature was significantly shorter for the cryogenic test (Figure 24) than the hypergolic test. The peak cryogenic temperatures occurred

between 0.1 and 1.0 sec after rupture, and the hypergolic peaks occurred from 1.3 to 1.9 sec after rupture. The static failure mode cryogenic test temperature curves were similar in time to peak-temperature to the cryogenic fall-back tests. The single static failure mode hypergolic test produced temperature curves with no definite peak values, but instead a very gradual rise and decay.

The calculated temperatures from the radiation measurements are presented in Table 7. Comparison of the calculated temperature values with the maximum measured temperature values indicated a emissivity factor of approximately 0.25 is required for agreement of the two temperature sources for the fall-back hypergolic tests. A comparison for the cryogenic tests indicated emissivity factors from 0.45 to 0.55 would adjust the thermal radiation temperature to equal the measured thermocouple temperatures in both the static and fall-back failure modes. No analysis was made for the static hypergolic test due to the low temperatures recorded from the thermocouples.

4.6.7 Calculated Overpressures

The results of the calculated overpressures using the shockwave velocity data and the Rankine-Hygoniot equation are given in Table 2 for the velocities which permit such an analysis. Since the Rankine-Hugoniot relationship permits accurate analysis only above approximately 5 psi, the N_2O_4/A-50 overpressures were not calculated. The cryogenic static failure mode test with a 0.1 sec delay also did not yield shock velocity which would permit analysis between the 25 and 40 ft gage stations.

4.6.8 Tankage Remains

The remains from three tests are shown in Figures 26, 27, and 28 to illustrate the type of tankage failure encountered during the program. The remains of a static failure mode hypergolic tests are shown in Figure 26. In this test the end (bottom) of the tank was blown off and the tank was projected in the air by the thrust from the burning propellants within the tank. It is significant that no

further damage was experienced by the tankage after the initial failure even though the propellants continued to react inside the tank. The static failure pressure of the tank was calculated as approximately 100 psi at the end joint of the tank.

The tankage fragments from static failure mode cryogenic tests are shown in Figure 27. The fragments in Figure 27 are only a portion of the total tankage, but due to the propellant reaction and brush-covered terrain around the test area these were the only ones recovered. Only a few small fragments from the fall-back failure mode cryogenic tankage were recovered from either test.

The remains of the lower section of a hypergolic fall-back tests are shown in Figure 28. The top of the upper tankage section was blown off, but little damage was observed for the rest of the section. Notice the size of the lower section fragments for this test condition compared to the fragments in the cryogenic test. The hypergolic propellant fragments are considerably larger and would indicate a slower reaction rate for the hypergolic propellants as compared to the cryogenic propellants. This slower rate results in the larger fragments.

5. CONCLUSIONS

Based on the results of the experimental studies conducted on this program, the following conclusions are made.

5.1 BLAST YIELD

The explosive yield of the LOX/RP-1 tests was considerably higher than the N_2O_4/A-50 tests in both the static and fall-back failure modes. The N_2O_4/A-50 tests indicates TNT overpressure and impulse equivalences of less than 0.01 lb of TNT per lb of propellant in both the static and fall-back failure modes. The cryogenic tests yielded TNT overpressure equivalences from less than 0.1 lb of TNT per lb of propellant for a short mixing delay time to between 0.07 and 0.05 lb of TNT per lb of propellant for a long

mixed sample in a static failure mode. The fall-back failure mode tests indicated TNT overpressure equivalences of 0.05 to 0.15 lb of TNT per lb of LOX/RP-1 propellant for a fall-back failure mode. A similar analysis of the impulse data indicated the LOX/RP-1 propellant test yielded 15 to 20 times the N_2O_4/A-50 impulse values in a fall-back failure mode.

The phenomena of partitioning of energy observed for previous studies (Reference 1) was not indicated by the test results for these limited studies.

It is possible to initiate the LOX/RP-1 propellant in aluminum tankage by impact alone and no stimuli such as an explosive charge in the tank was required. Cause of the spontaneous initiation was not determined, but the results were the same as observed in previous similar studies (Reference 1).

Although the same amount of propellants was used in these tests as was used in previous controlled mixing tests (Reference 1), the maximum blast yield (in peak overpressure) was 50 to 80 percent less in simulated tankage and demonstrates the important role of the mix conditions (contact area).

5.2 FIREBALL SIZE AND DURATION

The fireballs produced by the two propellants were essentially symmetrical and dependent on the failure mode of the tests and position of the tankage failure. The fall-back failure mode tankage tests with both the hypergolic and cryogenic propellants produced fireballs with small maximum heights due to the momentum of the propellants on impact. The cryogenic fall-back failure mode fireball diameters were approximately twice the hypergolic fireball diameters. The static failure mode tests did not indicate a definite trend except that the fireballs were smaller for the N_2O_4/A-50 propellant.

5.3 MAXIMUM TEMPERATURE

The hypergolic and cryogenic tests produced maximum temperatures of 3039°F and 2828°F respectively. The test results did not indicate a relationship between the fireball temperature and either the failure mode or the propellant.

5.4 THERMAL RADIATION YIELD

The thermal radiation data did not indicate a relationship between the total yield and either the propellant or the failure mode. A maximum yield of 2.3×10^9 joules was recorded from the cryogenic tests in a fall-back failure mode. The hypergolic tests produced a maximum yield of 1.19×10^8 in a static failure mode.

The fireball radiation data indicated emissivity values of 0.45 to 0.55 for the cryogenic tests and 0.25 for the hypergolic tests.

6. RECOMMENDATIONS

It is recommended that the results reported herein be recognized for their limitations and for the fact that they cannot be presently applied or extrapolated to conditions other than the propellant weight and test methods employed.

It is therefore recommended that additional tests of this nature and of larger magnitude be conducted if it is desirable to more accurately characterize the explosion hazards of the propellants.

REFERENCES

1. Blast and Fireball Comparison of Cryogenic and Hypergolic Propellants, Aerojet-General Corporation, Final Report 0822-01, Contract NAS 9-2055, June 1964.

2. Titan II - Dyna-Soar Destruct Test and Analysis Report, Martin-Marietta Corporation, Report ER 12269, Contract AF04(695)-54, 15 March 1962.

3. Evaluation of Radiant Heat Flux and Toxicity in Dyna-Soar-Titan II Destruct Tests, Bureau of Mines, Technical Documentary Report ASD-TDR-62-221, May 1962.

4. Summary Report on a Study of the Blast Effect of a Saturn Vehicle, A.D. Little, Inc., Report C-63850, Contract NAS 8-523, February 1962. (Confidential).

5. Explosive Potential of "ATLAS" Propellants, Broadview Research Corporation, Final Summary Report BRC-57-6A1, June 1957 (Confidential).

6. Titan II Propellant Hazards, Rocketdyne, Special Final Report R-2847, Contract AF33(616)-2939, 31 January 1964.

7. Kingery, C. and Pannil, B., Peak Overpressure vs Scaled Distance, BRL memo Report 1518, April 1964.

8. Kingery, C., Informal notes, Ballistic Research Laboratories, Aberdeen Proving Grounds, Maryland, (Being compiled for publication).

TABLE 1

PROPELLANT TEST PLAN*

Propellant	Failure Mode	Oxidizer/Fuel Weight Ratio**	Position of Propellant in Tankage	
			Lower Section	Upper Section
LOX/RP-1***	Static	2.5:1	LOX	RP-1
	Fall-Back	2.5:1	RP-1	LOX
N_2O_4/A-50****	Static	2:1	N_2O_4	A-50
	Fall-Back	2:1	A-50	N_2O_4

* Three hundred lb of propellant per test. Propellant contact area = 247 in.^{2}.

** Two tests for each condition. Eight tests total.

*** Propellant length to diameter ratio = 1.8:1.

**** Propellant length to diameter ratio = 1.6:1.

TABLE 2

SHOCK VELOCITIES AND CALCULATED OVERPRESSURES

Test No.	Propellant	Type of Test	Location Gage No.	to Gage No.	Average Velocity (ft/sec)	Calculated Overpressure (psi)
1	LOX/RP-1	Static (0.1 sec initiation delay)	1	5	1316	6.3
			2	6	1327	6.7
			3	7	1261	4.4
			4	8	1304	5.9
			5	9	1190	*
			6	10	1190	*
			7	11	1190	*
			8	12	1181	*
2	LOX/RP-1	Static (0.4 sec initiation delay)	1	5	2290	53.1
			2	6	2174	46.2
			3	7	2083	41.1
			4	8	2128	43.6
			5	9	1456	11.6
			6	10	1415	10.1
			7	11	1442	11.1
			8	12	1485	12.8
3	N_2O_4/A-50	Static	No data*			
4	N_2O_4/A-50	Static	No data*			
5	LOX/RP-1	Fall-Back	1	5	2222	47.0
			2	6	2326	53.1
			3	7	2439	60.0
			4	8	2344	54.1
			5	9	1546	14.2
			6	10	1500	12.4
			7	11	1546	14.2
			8	12	1563	14.9
6	LOX/RP-1	Fall-Back	1	5	2703	76.6
			2	6	2885	89.5
			3	7	2727	78.2
			4	8	2778	81.8
			5	9	1613	16.6
			6	10	1630	17.3
			7	11	1667	18.9
			8	12	1705	20.5
7	N_2O_4/A-50	Fall-Back	1	5	1154	*
			2	6	1293	
			3	7	1200	
			4	8	1181	
			5	9	1145	
			6	10	1154	
			7	11	1103	
			8	12	1154	
8	N_2O_4/A-50	Fall-Back	1	5	1200	*
			2	6	1282	
			3	7	1282	
			4	8	1230	
			5	9	1103	
			6	10	1177	
			7	11	1168	
			8	12	1181	

* Shockwave velocities too low to permit accurate analysis.

TABLE 3

BLAST RESULTS

Test No.	Propellant	Type of Test	Gage Position No.	Peak Overpressure (psi)	Positive Impulse (psi)	Positive Pulse Duration (msec)	Maximum Radiant Heat Flux (BTU/ft^2-sec)	Maximum Temperature (°F)
1	LOX/RP-1	Static (0.1 sec initiation delay)	1	8.2	9.4	2.6	50.0	2318
			2	10.8	12.0	4.1	75.0	2376
			3	7.4	11.3	3.1	38.0	2130
			4	6.8	11.0	3.2	25.0	1324
			Mean	8.3	10.9	3.3		
			5	2.7	4.7	4.6	25.0	422
			6	2.0	3.4	4.3	33.0	1213
			7	2.7	4.4	4.2	16.6	350
			8	2.8	4.7	4.2	11.0	229
			Mean	2.6	4.3	4.3		
			9	1.3	2.9	3.8	No data	229
			10	1.1	2.4	4.9	8.5	228
			11	1.3	2.3	4.0	7.4	228
			12	1.0	2.3	5.0	5.0	Ambient
			Mean	1.2	2.5	4.4		
2	LOX/RP-1	Static (0.4 sec initiation delay)	1	88.0	*	*	83.7	2681
			2	75.3	*	*	89.3	2222
			3	*	*	*	68.7	2627
			4	*	*	*	45.1	2129
			Mean	81.7				
			5	10.8	35.7	8.0	47.1	2028
			6	10.3	31.7	6.4	41.8	1491
			7	12.4	36.9	6.2	25.9	572
			8	6.7	*	5.1	25.8	315
			Mean	10.1	34.8	6.4		
			9	4.5	25.1	12.2	15.1	289
			10	2.2	10.6	10.2	16.6	322
			11	6.0	20.9	7.0	9.8	255
			12	3.6	14.7	6.5	7.4	424
			Mean	4.1	17.8	9.0		
3	N_2O_4/A-50	Static	1	**	**	**	24.8	***
			2	**	**	**	26.5	
			3	**	**	**	18.7	
			4	**	**	**	20.8	
			Mean					
			5	**	**	**	7.5	
			6	**	**	**	4.9	
			7	**	**	**	3.3	
			8	**	**	**	3.2	
			Mean					
			9	**	**	**	1.7	
			10	**	**	**	1.8	
			11	**	**	**	1.6	
			12	**	**	**	1.4	
			Mean					

TABLE 3

Continued

Test No.	Propellant	Type of Test	Gage Position No.	Peak Overpressure (psi)	Positive Impulse (psi)	Positive Pulse Duration (msec)	Maximum Radiant Heat Flux (BTU/ft^2-sec)	Maximum Temperature (^{o}F)
4	N_2O_4/A-50	Static	1	0.5	****	2.9	12.1	648
			2	0.5	****	3.2	13.0	973
			3	0.5	****	3.2	2.7	Ambient
			4	0.6	****	3.8	3.0	Ambient
			Mean	0.5		3.3		
			5	0.3	****	5.1	3.4	Ambient
			6	0.2	****	4.5	5.3	836
			7	0.2	****	4.5	1.3	Ambient
			8	0.2	****	5.0	1.8	Ambient
			Mean	0.2		4.8	-	
			9	0.4	****	5.4	1.1	Ambient
			10	0.1	****	5.0	1.4	Ambient
			11	0.1	****	4.4	0.8	Ambient
			12	0.1	****	3.6	0.7	Ambient
			Mean	0.2		4.6		
5	LOX/RP-1	Fall-Back	1	55.3	96.7	6.5	16.5	>339
			2	53.9	*	*	34.9	>845
			3	56.6	121.2	3.7	66.7	1905
			4	*	*	*	18.2	>679
			Mean	55.3	109.0	5.1		
			5	17.3	37.1	6.0	17.2	1010
			6	16.5	34.1	5.8	25.5	959
			7	26.4	57.8	6.7	41.7	2176
			8	21.0	36.9	5.0	17.4	1168
			Mean	20.3	41.5	5.9		
			9	7.5	28.4	11.0	43.9	2574
			10	6.4	22.6	8.2	30.6	1897
			11	9.2	28.9	8.2	23.0	1200
			12	7.4	23.3	6.3	>12.2	1479
			Mean	7.6	25.8	8.4		
6	LOX/RP-1	Fall-Back	1	72.9	109.1	3.8	66.1	2020
			2	41.0	84.4	3.3	103.7	*
			3	51.3	142.5	4.4	129.2	2828
			4	50.3	105.6	4.9	104.0	1897
			Mean	53.9	110.4	4.1		
			5	20.1	62.9	6.9	36.5	1219
			6	18.0	44.2	6.4	54.9	2352
			7	18.0	53.6	5.8	57.0	1345
			8	16.8	31.4	4.7	60.5	>2678
			Mean	18.2	48.0	6.0		
			9	8.1	42.5	10.5	50.0	2789
			10	6.9	28.1	7.5	27.8	*
			11	8.2	29.9	6.7	37.4	1347
			12	8.9	32.3	10.5	22.9	>1922
			Mean	8.0	33.2	8.8		

TABLE 3

Continued

Test No.	Propellant	Type of Test	Gage Position No.	Peak Overpressure (psi)	Positive Impulse (psi)	Positive Pulse Duration (msec)	Maximum Radiant Heat Flux (BTU/ft^2-sec)	Maximum Temperature (^oF)
7	N_2O_4/A-50	Fall-Back	1	1.8	5.4	6.0	10.6	1197
			2	9.7	12.1	4.6	36.7	2920
			3	8.2	9.3	3.1	26.7	2280
			4	2.0	6.2	8.1	11.1	445
			Mean	5.4	8.3	5.5		
			5	0.8	2.0	5.4	9.9	1241
			6	2.1	3.6	4.3	35.2	2618
			7	2.5	5.8	7.1	8.5	361
			8	1.0	2.1	4.0	5.7	250
			Mean	1.6	3.4	5.2		
			9	0.5	1.6	6.0	2.6	194
			10	1.0	2.1	4.5	17.8	1708
			11	1.1	2.2	4.9	4.3	210
			12	0.6	1.3	5.5	2.4	185
			Mean	0.8	1.8	5.2		
8	N_2O_4/A-50	Fall-Back	1	3.0	10.4	6.8	11.8	2017
			2	10.1	13.0	3.8	32.8	2844
			3	17.0	21.7	3.6	36.6	3039
			4	5.0	10.2	5.0	8.3	386
			Mean	8.8	13.8	4.8		
			5	1.3	5.4	7.5	6.9	218
			6	3.6	6.6	4.4	25.0	2106
			7	4.8	7.7	4.5	14.6	779
			8	2.8	5.0	4.1	4.0	203
			Mean	3.1	6.2	5.1		
			9	0.8	3.3	8.3	1.4	178
			10	1.9	4.2	4.8	4.9	203
			11	2.5	4.7	5.1	4.1	194
			12	1.5	2.9	5.0	1.8	178
			Mean	1.7	3.8	5.8		

* Gage damaged by tank fragments.

** Peak overpressure, positive impulses and pulse durations were insufficient to warrant measurement. Overpressures were less than 0.1 psi at all stations.

*** No accurate temperature data obtained due to malfunction of oscillograph recording system.

**** No positive impulse values were determined due to the low overpressure valves.

TABLE 4

FIREBALL DATA

Propellant	Test No.	Failure Mode	Maximum Height (ft)	Maximum Diameter (ft)	Duration (sec)	Total Yield (Joules)
LOX/RP-1	1	Static	95	67	3.22	3.0×10^8
	2	Static	90	85	3.25	3.4×10^8
N_2O_4/A-50	3	Static	81	53	2.73	1.19×10^8
	4	Static	23	30	3.20*	9.30×10^7
LOX/RP-1	5	Fall-Back	35	117	2.00	2.3×10^9
	6	Fall-Back	38	113	2.46	7.3×10^6
N_2O_4/A-50	7	Fall-Back	35	51	3.68	9.6×10^7
	8	Fall-Back	32	55	4.20	6.7×10^7

* Reignited 2.0 seconds after termination of initial fireball and burned for an undetermined period.

TABLE 5

FIREBALL SPECTRAL DISTRIBUTION AND INTENSITY - LOX/RP-1.

Failure Mode	Test No.	Time (sec)	0.4 to 0.7 μ Wavelength	0.7 to 1.1 μ Wavelength	1.8 to 2.7 μ Wavelength	3 to 5 μ Wavelength	0.5 to 35 μ Wavelength
Static	1	0.1	*	**	4.00×10^5	6.30×10^5	2.70×10^6
		0.2			8.10×10^5	1.09×10^5	5.50×10^6
		0.3			1.02×10^6	1.25×10^5	6.40×10^6
		0.4			1.20×10^6	1.39×10^5	7.10×10^6
		0.5			1.30×10^6	1.46×10^5	7.55×10^6
		0.6			1.38×10^6	1.51×10^5	8.00×10^6
		0.7			1.46×10^6	1.57×10^5	8.20×10^6
		0.8			1.54×10^6	1.61×10^5	8.40×10^6
		0.9			1.57×10^6	1.63×10^5	8.90×10^6
		1.0			1.65×10^6	1.65×10^5	9.25×10^6
		1.1			1.75×10^6	1.70×10^5	9.40×10^7
		1.2			1.85×10^5	1.81×10^5	1.04×10^7
		1.3			1.88×10^6	1.80×10^5	1.05×10^7
		1.4			1.79×10^6	1.77×10^5	1.02×10^7
		1.5			1.63×10^6	1.66×10^5	4.60×10^6
		1.6			1.33×10^6	1.42×10^5	7.80×10^6
		1.7			1.02×10^6	1.21×10^5	7.00×10^6
		1.8			7.60×10^5	1.06×10^6	5.80×10^6
		1.9			5.00×10^5	7.80×10^5	4.30×10^6
		2.0			3.40×10^5	5.00×10^5	3.05×10^6
		2.1			2.30×10^5	3.10×10^5	2.15×10^6
		2.2				1.93×10^5	1.79×10^6
		2.3				1.21×10^5	1.26×10^6
Static	2	0.1	2.1×10^4	1.26×10^5	8.20×10^5	5.60×10^5	4.10×10^6
		0.2	2.9×10^4	2.60×10^5	1.64×10^6	1.38×10^6	9.30×10^6
		0.3	3.2×10^4	3.40×10^5	2.10×10^6	1.95×10^6	1.35×10^7
		0.4	3.8×10^4	3.60×10^5	2.30×10^6	2.10×10^6	1.58×10^7
		0.5	4.7×10^4	4.00×10^5	2.40×10^6	2.30×10^6	1.59×10^7
		0.6	4.2×10^4	3.80×10^5	2.40×10^6	2.40×10^6	1.61×10^7
		0.7	3.7×10^4	3.50×10^5	2.40×10^6	2.40×10^6	1.60×10^7
		0.8	3.2×10^4	3.10×10^5	2.30×10^6	2.30×10^6	1.58×10^7
		0.9	2.8×10^4	2.80×10^5	2.30×10^6	2.25×10^6	1.46×10^7
		1.0	2.9×10^4	2.60×10^5	2.30×10^6	2.20×10^6	1.43×10^7
		1.1	-	-	2.20×10^6	2.10×10^6	1.36×10^7
		1.2	2.60×10^4	2.40×10^5	2.10×10^6	1.91×10^6	1.20×10^7
		1.3	-		1.85×10^6	1.56×10^6	1.03×10^6
		1.4	2.10×10^4	2.00×10^5	1.62×10^6	1.26×10^6	8.50×10^6
		1.5	-		1.29×10^5	9.10×10^5	6.30×10^6
		1.6	1.83×10^4	1.72×10^5	9.60×10^5	6.20×10^5	4.60×10^6
		1.7	-		6.40×10^5	4.10×10^5	3.05×10^6
		1.8	1.32×10^4	1.23×10^5	4.10×10^5	2.70×10^5	1.93×10^6
		1.9	-		2.50×10^5	1.52×10^5	1.40×10^6
		2.0	1.57×10^4	9.60×10^4	1.64×10^5	1.28×10^5	1.29×10^6
Fall-Back	5	0.1	5.10×10^4	3.50×10^5	1.32×10^6	1.04×10^6	8.90×10^6
		0.2	5.70×10^4	4.90×10^5	2.03×10^6	1.84×10^6	1.55×10^7
		0.3	5.30×10^4	4.70×10^5	$2,08 \times 10^6$	1.99×10^6	1.56×10^7
		0.4	4.50×10^4	4.00×10^5	2.07×10^6	2.00×10^6	1.53×10^7
		0.5	4.00×10^4	3.33×10^5	2.01×10^6	1.95×10^6	1.43×10^7
		0.6	3.60×10^4	3.20×10^5	1.90×10^6	1.90×10^6	1.33×10^7
		0.7	2.60×10^4	2.30×10^5	1.81×10^6	1.84×10^6	1.20×10^7
		0.8	2.90×10^4	2.00×10^5	1.68×10^6	1.73×10^6	1.13×10^7
		0.9	2.50×10^4	1.83×10^5	1.61×10^6	1.63×10^6	1.04×10^7
		1.0	2.50×10^4	1.63×10^5	1.46×10^6	1.50×10^6	9.70×10^6
		1.2	1.59×10^4	1.08×10^4	1.15×10^5	1.14×10^6	6.70×10^6
		1.4	1.59×10^4	8.80×10^4	7.80×10^5	8.00×10^5	4.80×10^6
		1.6	1.45×10^4	5.00×10^4	4.80×10^5	5.20×10^5	3.10×10^6
		1.8	1.64×10^4	5.40×10^4	3.00×10^5	3.40×10^5	2.00×10^6
		2.0	1.22×10^4	4.20×10^4			1.48×10^6

TABLE 5

Continued

Failure Mode	Test No.	Time (sec)	0.4 to 0.7 μ Wavelength	0.7 to 1.1 μ Wavelength	1.8 to 2.7 μ Wavelength	3 to 5 μ Wavelength	0.5 to 35 μ Wavelength
Fall-Back	6	0.1	1.44×10^{5}	1.09×10^{6}	3.10×10^{6}	2.60×10^{6}	2.40×10^{7}
		0.2	1.12×10^{4}	9.10×10^{5}	3.20×10^{6}	2.90×10^{6}	2.40×10^{7}
		0.3	8.20×10^{4}	7.00×10^{5}	3.00×10^{6}	2.70×10^{6}	2.10×10^{7}
		0.4	5.60×10^{4}	5.00×10^{5}	2.80×10^{6}	2.50×10^{6}	1.84×10^{7}
		0.5	4.50×10^{4}	4.20×10^{5}	2.50×10^{6}	2.40×10^{6}	1.58×10^{7}
		0.6	3.90×10^{4}	2.80×10^{5}	2.30×10^{6}	2.20×10^{6}	1.42×10^{7}
		0.7	3.00×10^{4}	2.40×10^{5}	2.20×10^{6}	2.10×10^{6}	1.30×10^{7}
		0.8	2.40×10^{4}	2.10×10^{5}	2.00×10^{6}	1.93×10^{6}	1.18×10^{7}
		0.9	2.15×10^{4}	1.82×10^{5}	1.93×10^{6}	1.86×10^{6}	1.12×10^{7}
		1.0	2.19×10^{4}	1.57×10^{5}	1.82×10^{6}	1.71×10^{6}	1.04×10^{7}
		1.2	1.61×10^{4}	1.06×10^{5}	1.42×10^{6}	1.33×10^{5}	8.00×10^{6}
		1.4	1.34×10^{4}	9.10×10^{4}	1.00×10^{5}	9.50×10^{5}	5.30×10^{6}
		1.6	1.21×10^{4}	6.20×10^{3}	6.70×10^{5}	6.10×10^{5}	3.70×10^{6}
		1.8	6.30×10^{3}	9.80×10^{3}	3.10×10^{5}	3.20×10^{5}	2.50×10^{6}
		2.0	5.40×10^{3}	8.70×10^{3}	2.20×10^{5}	2.30×10^{5}	2.10×10^{6}

* Signal was slightly above the sunlit terrain intensity. The background intensity was approximately 1×10^{4} w/steradian.

** Signal was slightly above the sunlit terrain intensity. The background intensity was approximately 4×10^{4} w/steradian.

TABLE 6

FIREBALL SPECTRAL DISTRIBUTION AND INTENSITY - N_2O_4/A-50.

Failure Mode	Test No.	Time (Sec)	0.4 to 0.7 μ Wavelength	0.7 to 1.1 μ Wavelength	1.8 to 2.7 μ Wavelength	3 to 5 μ Wavelength	0.5 to 35 μ Wavelength
Static	3	0.1	*	**	3.20×10^5	2.40×10^5	1.34×10^6
		0.2			4.80×10^5	3.70×10^5	1.81×10^6
		0.3			5.05×10^5	4.10×10^5	2.00×10^6
		0.4			5.30×10^5	4.50×10^5	2.10×10^6
		0.5			5.30×10^5	4.40×10^5	2.15×10^6
		0.6			5.40×10^5	4.60×10^5	2.30×10^6
		0.7			5.55×10^5	4.70×10^5	2.40×10^6
		0.8			5.70×10^5	4.90×10^5	2.60×10^6
		0.9			5.90×10^5	5.00×10^5	2.75×10^6
		1.0			6.30×10^5	5.20×10^5	3.20×10^6
		1.1			7.60×10^5	6.20×10^5	3.70×10^6
		1.2			8.10×10^5	6.40×10^5	4.30×10^6
		1.3			8.50×10^5	5.95×10^5	4.50×10^6
		1.4			8.45×10^5	5.00×10^5	4.50×10^6
		1.5			8.00×10^5	3.80×10^5	4.45×10^6
		1.6			7.00×10^5	2.85×10^5	3.40×10^6
		1.7			5.55×10^5	1.68×10^5	3.10×10^6
		1.8			4.30×10^5	1.17×10^5	2.22×10^6
		1.9			3.15×10^5	8.65×10^4	1.81×10^6
		2.0			2.00×10^5	-	1.53×10^6
		2.1			1.33×10^5	-	9.20×10^5
		2.2			8.30×10^4	-	7.30×10^5
Static	4	0.1	*	**	3.90×10^4	4.10×10^4	4.00×10^5
		0.2			6.20×10^4	5.60×10^4	5.40×10^5
		0.3			7.80×10^4	7.90×10^4	6.50×10^5
		0.4			9.30×10^4	9.50×10^4	6.50×10^5
		0.5			1.09×10^5	1.10×10^5	7.50×10^5
		0.6			1.29×10^5	1.24×10^5	6.80×10^5
		0.7			1.32×10^5	1.37×10^5	1.00×10^6
		0.8			1.59×10^5	1.55×10^5	1.10×10^6
		0.9			1.63×10^5	1.64×10^5	1.07×10^6
		1.0			1.76×10^5	1.73×10^5	1.08×10^6
		1.2			2.06×10^5	1.91×10^5	1.40×10^6
		1.4			2.60×10^5	2.30×10^5	1.54×10^6
		1.6			3.00×10^5	2.30×10^4	1.94×10^6
		1.8			3.10×10^5	2.07×10^4	2.05×10^6
		2.0			3.10×10^5	1.76×10^4	2.00×10^6
		2.2			2.80×10^5	1.51×10^4	1.96×10^6
		2.4			2.40×10^5	1.40×10^4	1.56×10^6
		2.6			1.98×10^5	1.13×10^4	1.47×10^6
		2.8			1.51×10^5	8.10×10^4	1.10×10^6
		3.0			1.17×10^5	6.10×10^4	1.03×10^6
		3.2			7.60×10^4	5.00×10^4	6.50×10^5
		3.4			5.20×10^4	3.80×10^4	5.80×10^5
		3.6			5.20×10^4		6.50×10^5
		5.6			1.30×10^5		6.80×10^5
		5.8			1.59×10^5		7.00×10^5
		6.0			1.77×10^5		9.80×10^5
		6.2			1.95×10^5		9.80×10^5
		6.4			2.00×10^5		1.07×10^6
		6.6			1.98×10^5		8.20×10^5
		6.8			1.92×10^5		8.80×10^5
		7.0			1.82×10^5		9.30×10^5
		7.2			1.33×10^5		6.50×10^5
		7.4			9.40×10^4		5.80×10^5
		7.6			5.70×10^4		4.70×10^5
		7.8			3.60×10^4		5.10×10^5

TABLE 6

Continued

Failure Mode	Test No.	Time (Sec)	0.4 to 0.7 μ Wavelength	0.7 to 1.1 μ Wavelength	1.8 to 2.7 μ Wavelength	3 to 5 μ Wavelength	0.5 to 35 μ Wavelength
Fall-Back	7	0.1	*	**	2.60×10^5	2.10×10^5	1.65×10^6
		0.2			3.40×10^5	2.50×10^5	2.12×10^6
		0.3			3.50×10^5	2.90×10^5	2.30×10^6
		0.4			3.90×10^5	3.20×10^5	2.60×10^6
		0.5			4.20×10^5	3.60×10^5	2.70×10^6
		0.6			4.20×10^5	3.70×10^5	2.70×10^6
		0.7			4.40×10^5	4.00×10^5	2.80×10^6
		0.8			4.70×10^5	4.00×10^5	2.90×10^6
		0.9			4.70×10^5	4.10×10^5	3.00×10^6
		1.0			4.80×10^5	4.40×10^5	3.10×10^6
		1.2			5.20×10^5	4.50×10^5	3.30×10^6
		1.4			5.30×10^5	4.80×10^5	3.40×10^6
		1.6			5.20×10^5	4.90×10^5	3.50×10^6
		1.8			4.70×10^5	4.20×10^5	3.20×10^6
		2.0			4.10×10^5	3.90×10^5	2.90×10^6
		2.2			3.50×10^5	3.20×10^5	2.40×10^6
		2.4			2.50×10^5	2.50×10^5	2.00×10^6
		2.6			1.40×10^5	1.86×10^5	1.83×10^6
		2.8			9.90×10^4	1.05×10^5	9.85×10^5
		3.0			7.30×10^4	9.00×10^4	7.90×10^5
Fall-Back	8	0.1	*	**	1.66×10^5	1.42×10^5	1.24×10^6
		0.2			2.08×10^5	1.74×10^5	1.50×10^6
		0.3			2.20×10^5	1.80×10^5	1.67×10^6
		0.4			2.30×10^5	1.96×10^5	2.03×10^6
		0.5			2.80×10^5	2.40×10^5	1.98×10^6
		0.6			2.90×10^5	2.60×10^5	2.03×10^6
		0.7			3.00×10^5	2.80×10^5	2.03×10^6
		0.8			3.00×10^5	2.70×10^5	2.10×10^6
		0.9			3.10×10^5	3.00×10^5	2.40×10^6
		1.0			3.40×10^5	3.30×10^5	2.40×10^6
		1.2			3.40×10^5	3.20×10^5	2.50×10^6
		1.4			3.40×10^5	3.40×10^5	2.60×10^6
		1.6			3.30×10^5	3.20×10^5	2.40×10^6
		1.8			3.00×10^5	2.90×10^5	2.30×10^6
		2.0			2.50×10^5	2.50×10^5	1.98×10^6
		2.2			1.88×10^5	1.93×10^5	1.49×10^6
		2.4			9.10×10^4	1.82×10^5	9.30×10^5
		2.6			6.90×10^4	9.40×10^4	7.00×10^5
		2.8			4.70×10^4	6.20×10^4	6.50×10^5

* Signal was slightly above the sunlit terrain intensity. The background intensity was approximately 1×10^4 w/steradian.

** Signal was slightly above the sunlit terrain intensity. The background intensity was approximately 4×10^4 w/steradian.

TABLE 7

CALCULATED FIREBALL TEMPERATURE

Propellant	Failure Mode	Test No.	Fireball Area (ft^2)	Peak Intensity (w/steradian)	T, ^oK
LOX/RP-1	Static	1	3060	1.05×10^7	1200
LOX/RP-1	Static	2	3450	1.61×10^7	1290
LOX-RP-1	Fall-Back	5	2610	1.56×10^7	1370
LOX-RP-1	Fall-Back	6	2640	2.40×10^7	1530
N_2O_4/A-50	Static	3	2090	4.50×10^6	1890
N_2O_4/A-50	Static	4	85	2.05×10^6	1090
N_2O_4/A-50	Fall-Back	7	694	3.50×10^6	1320
N_2O_4/A-50	Fall-Back	8	1041	2.60×10^6	1100

Temperature correction factors–

$\epsilon = 0.75$, multiply T by 1.07
$\epsilon = 0.50$, multiply T by 1.19
$\epsilon = 0.25$, multiply T by 1.41

TABLE 8

METEOROLOGICAL DATA

Test No.	Propellant	Failure Mode	Air Temp (°F)	Relative Humidity (%)	Atmos. Pressure (in. of Hg)	Wind Velocity (mph)	Wind Direction
1	LOX/RP-1	Static	66	48	28.72	6-9	Northeast
2	LOX/RP-1	Static	57	68	28.80	4-9	Northeast
3	N_2O_4/A-50	Static	62	46	28.75	6-10	Northeast
4	N_2O_4/A-50	Static	62	57	28.77	4-7	Northeast
5	LOX/RP-1	Fall-Back	73	40	28.80	5-7	North
6	LOX/RP-1	Fall-Back	78	41	28.82	3-5	Northeast
7	N_2O_4/A-50	Fall-Back	74	46	28.82	2-6	North
8	N_2O_4/A-50	Fall-Back	75	40	28.85	0-4	Northeast

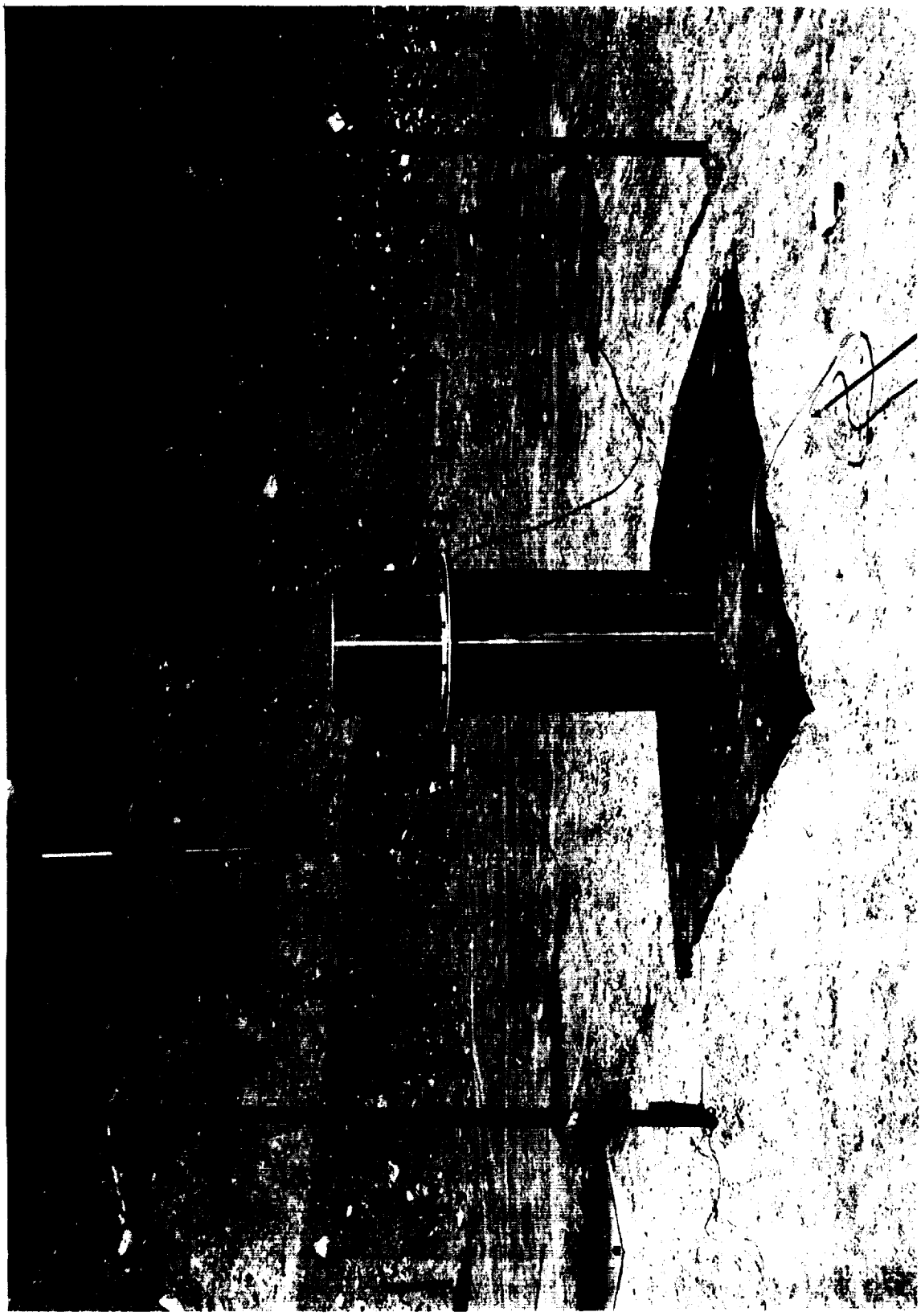

Figure 1. Typical Static Failure Mode Tank.

Figure 2. Propellant Test Area - Static Failure Mode.

Figure 3. Cryogenic Static Failure Mode Tankage With Insulated Lower Section.

BLACK AND WHITE PHOTOGRAPH

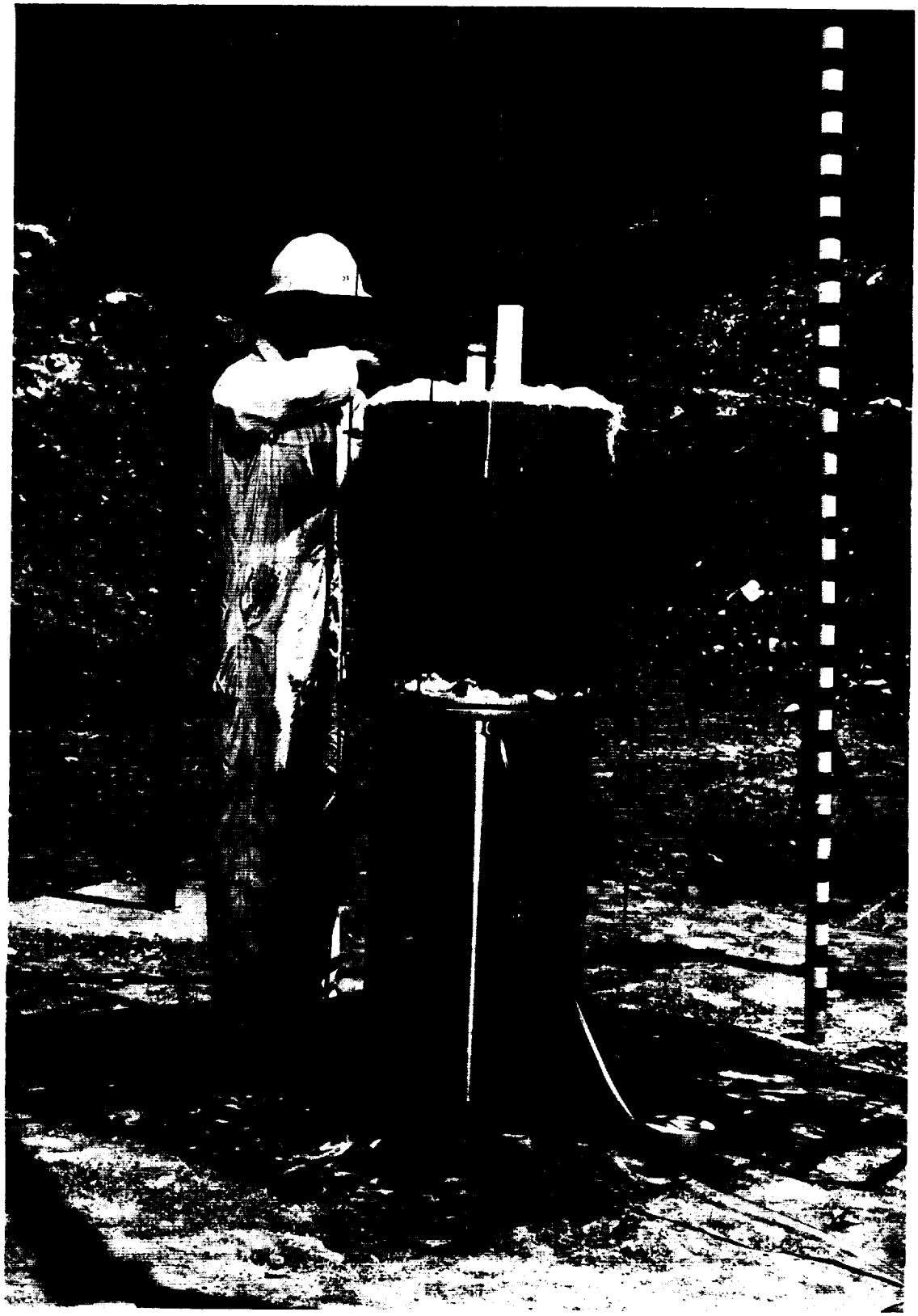

Figure 5. Cryogenic Fall-Back Failure Mode Tankage.

Figure 6. Hypergolic Fall-Back Tankage.

Figure 4. Static Failure Mode Diaphragm and Rupture Charge.

BLACK AND WHITE PHOTOGRAPH

Figure 8. Cryogenic Fall-Back Failure Mode Tankage in Drop Position.

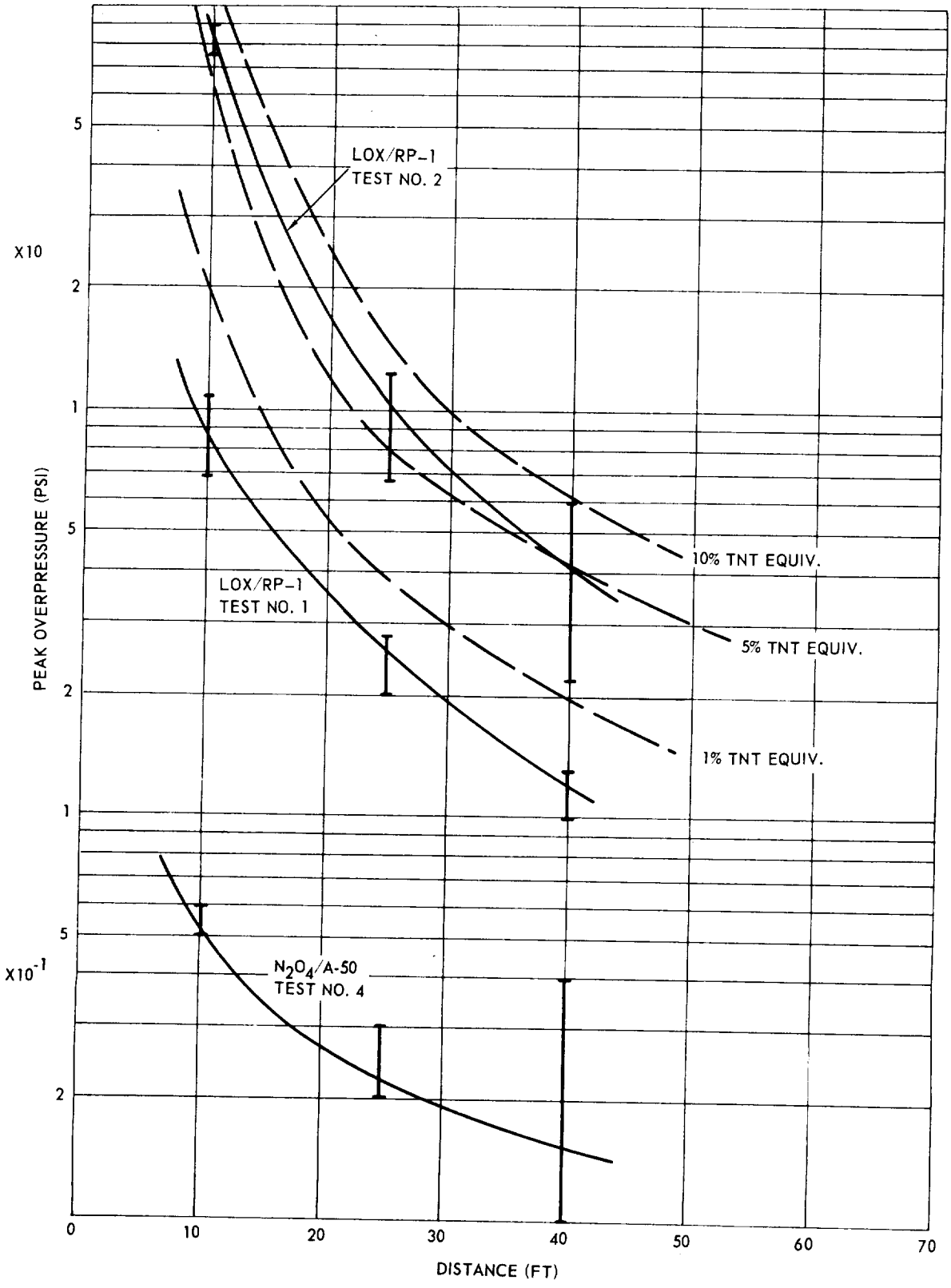

Figure 9. Peak Overpressure Data, Static Failure Mode. 300 lb Sample; 247 in.^{2} Contact Area

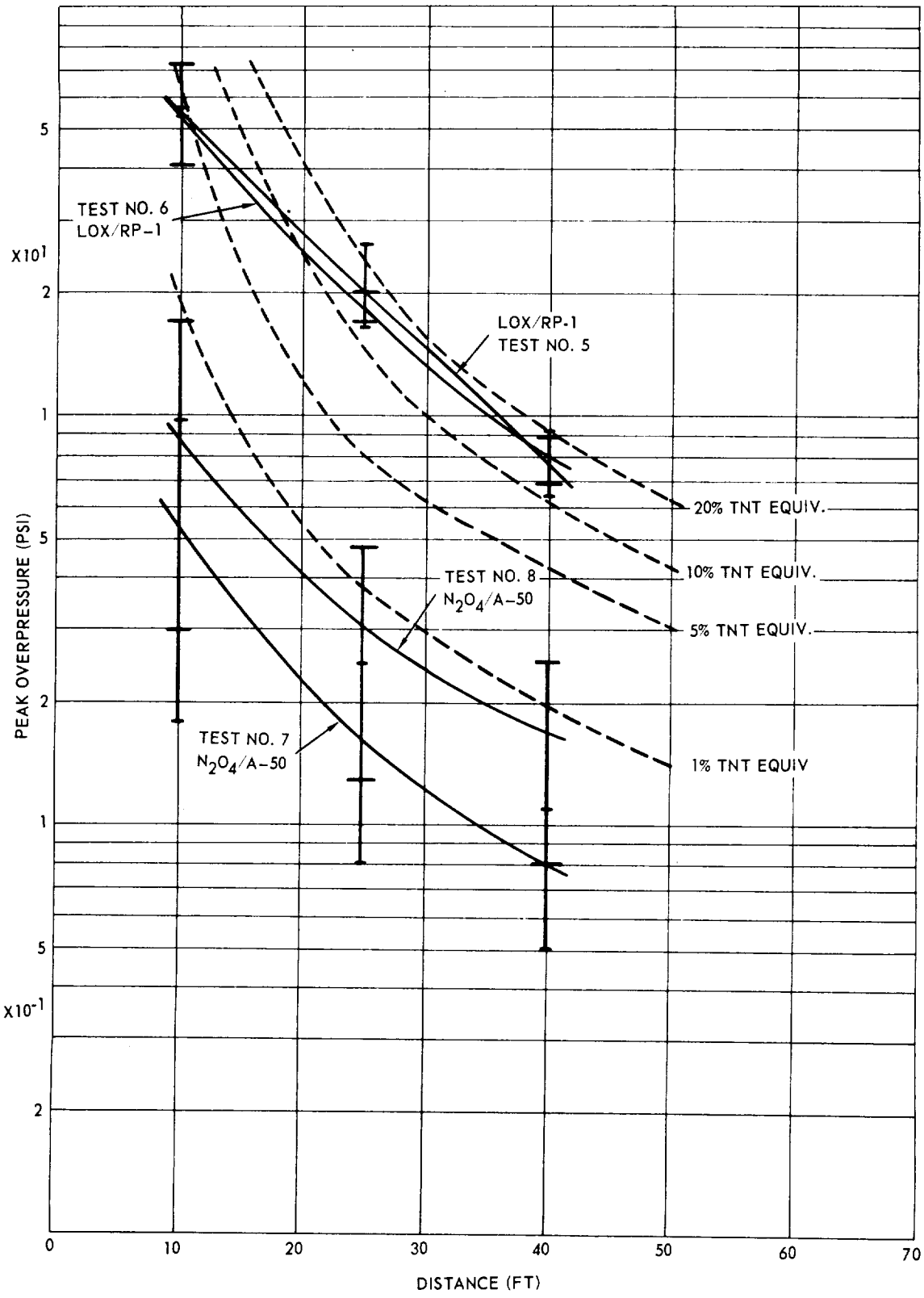

Figure 10. Peak Overpressure Data, Fall-Back Failure Mode. 300 lb Sample; 247 in.^{2} Contact Area

Figure 7. Cryogenic Fall-Back Failure Mode Tankage and Drop Tower.

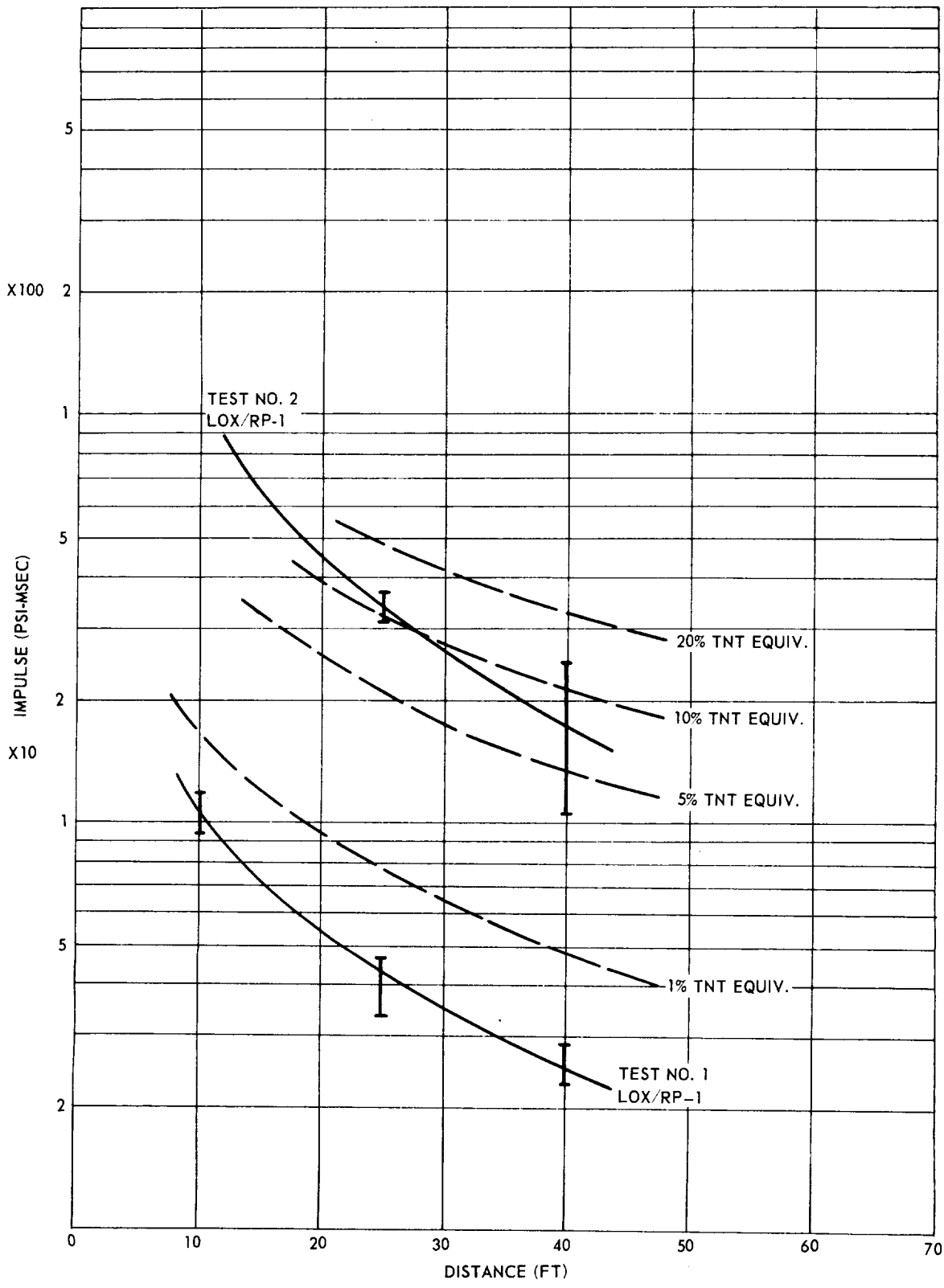

Figure 11. Positive Impulse Data, Static Failure Mode. 300 lb Sample; 247 in.^{2} Contact Area

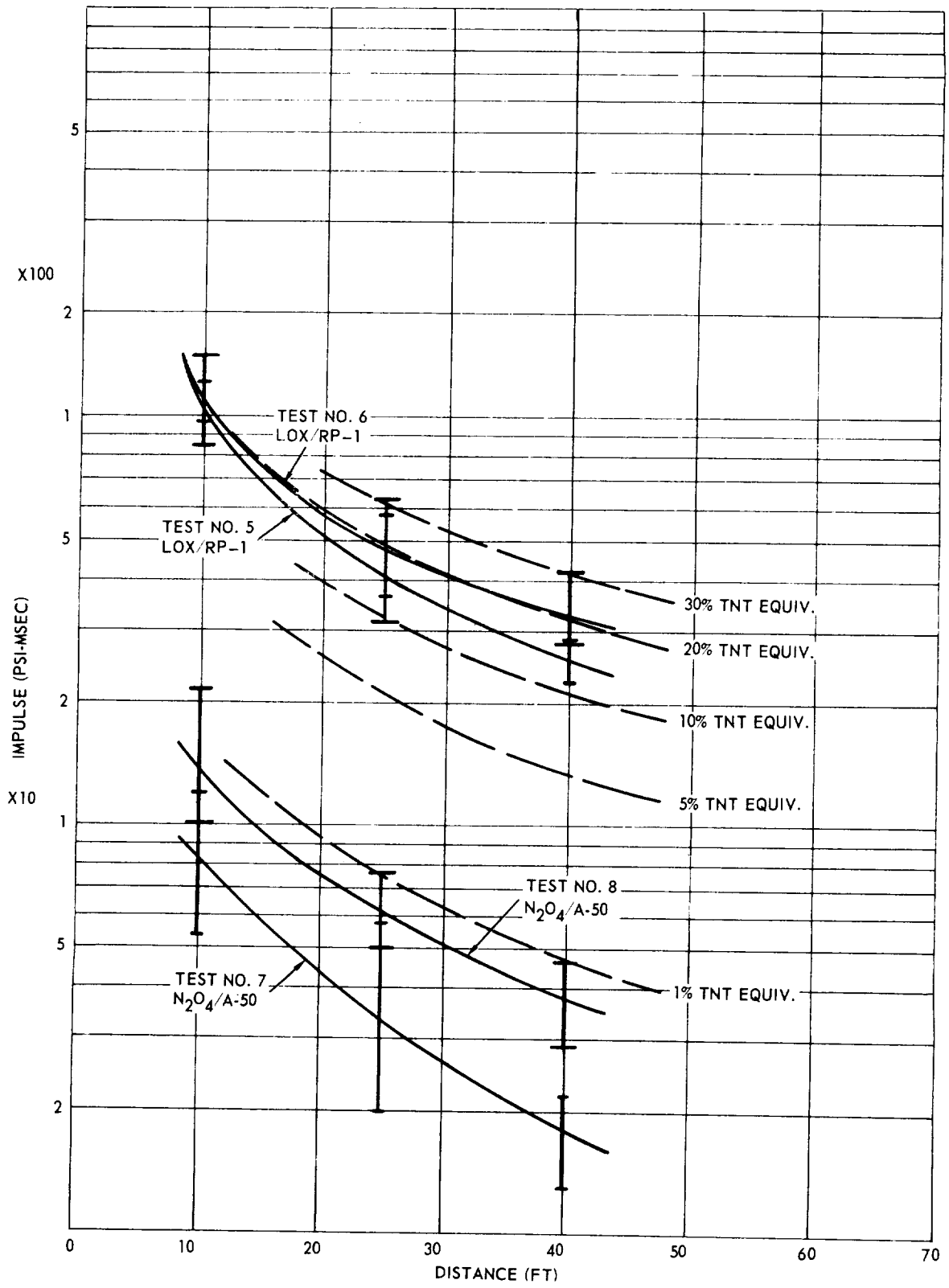

Figure 12.- Positive Impulse Data, Fall-Back Failure Mode. 300 lb Sample; 247 in.^{2} Contact Area

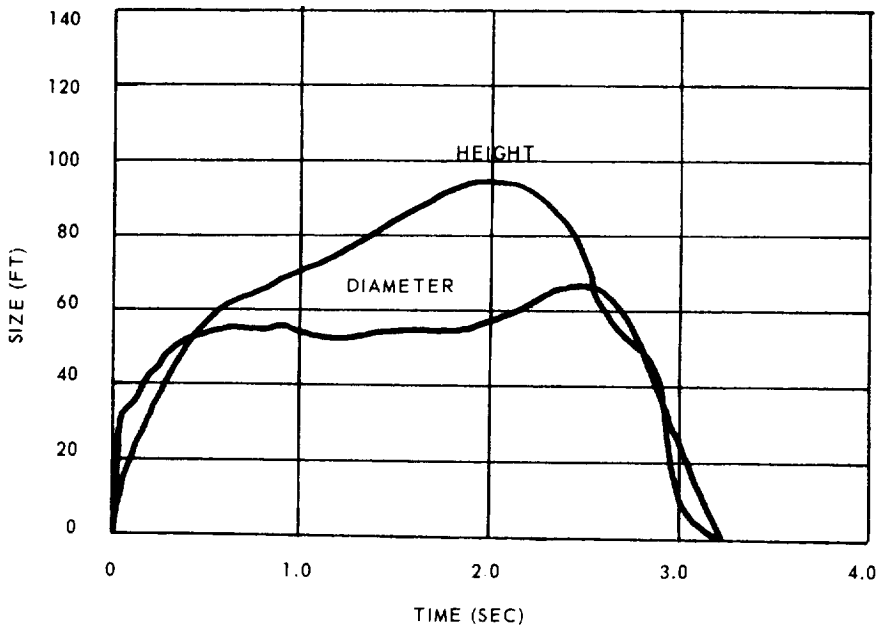

Test No. 1

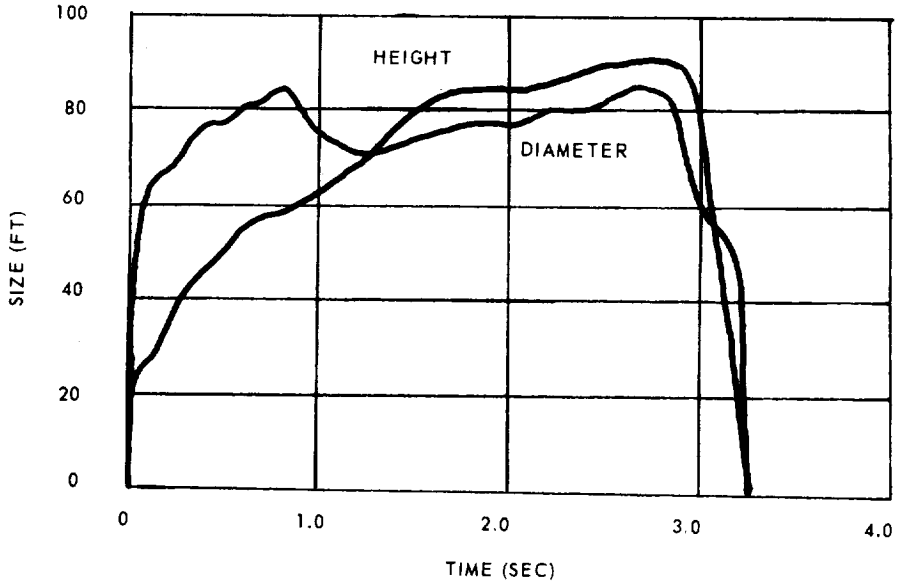

Test No. 2

Figure 13. Fireball History - LOX/RP-1 with Static Tankage.

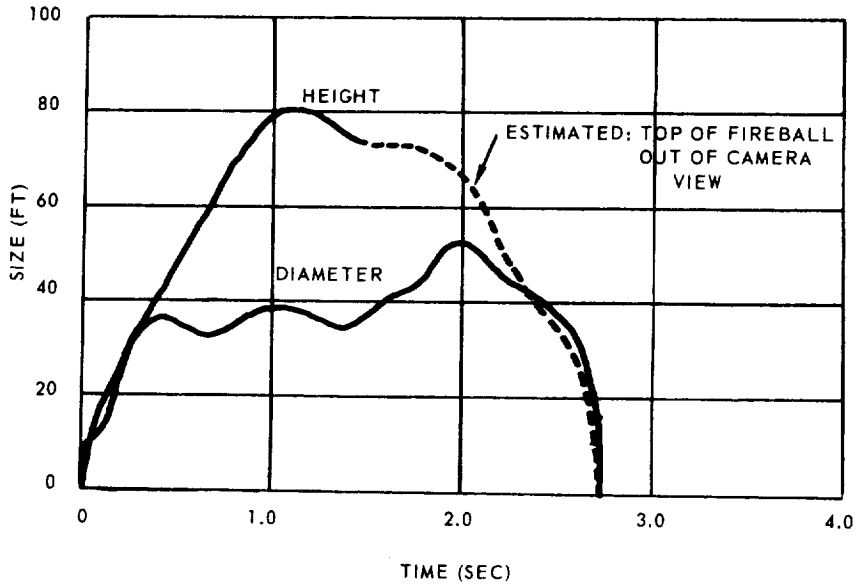

Test No. 3

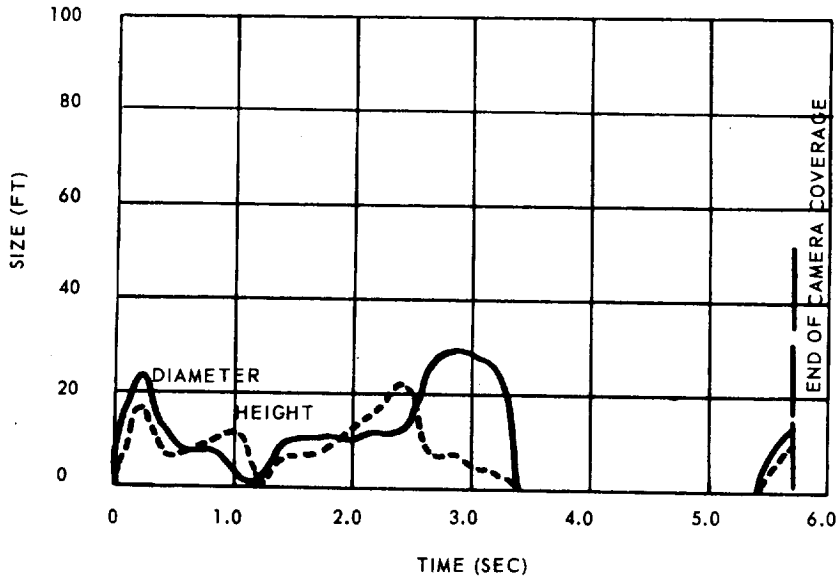

Test No. 4

Figure 14. Fireball History - N_2O_4/A-50 with Static Tankage.

Figure 15. N_2O_4/A-50 Fireball - Static Tankage.

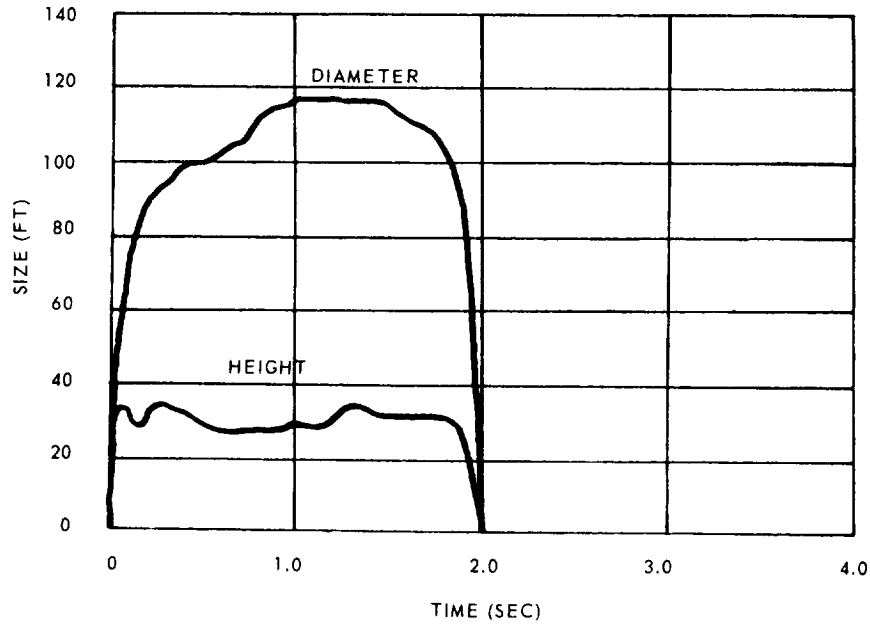

Test No. 5

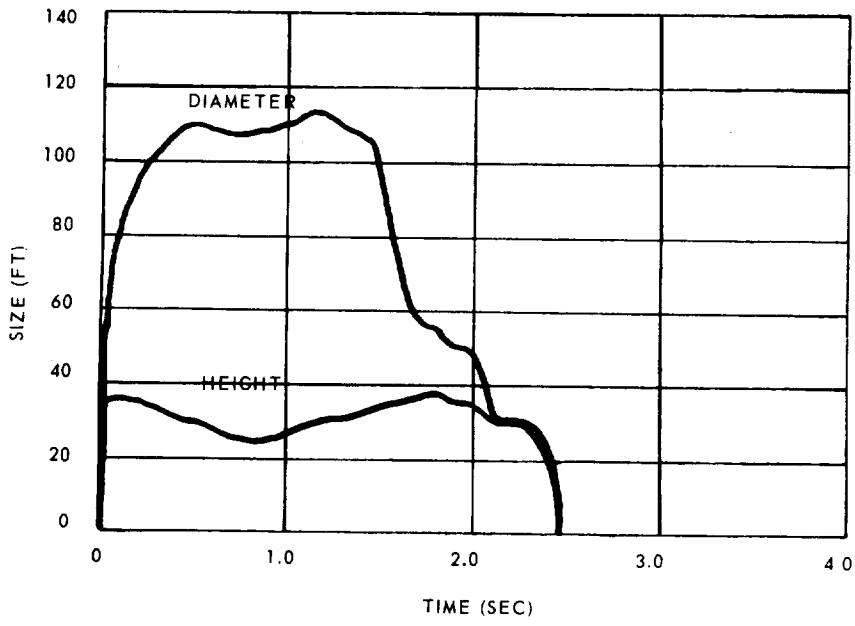

Test No. 6

Figure 16. Fireball History - LOX/RP-1 with Fall-Back Tankage.

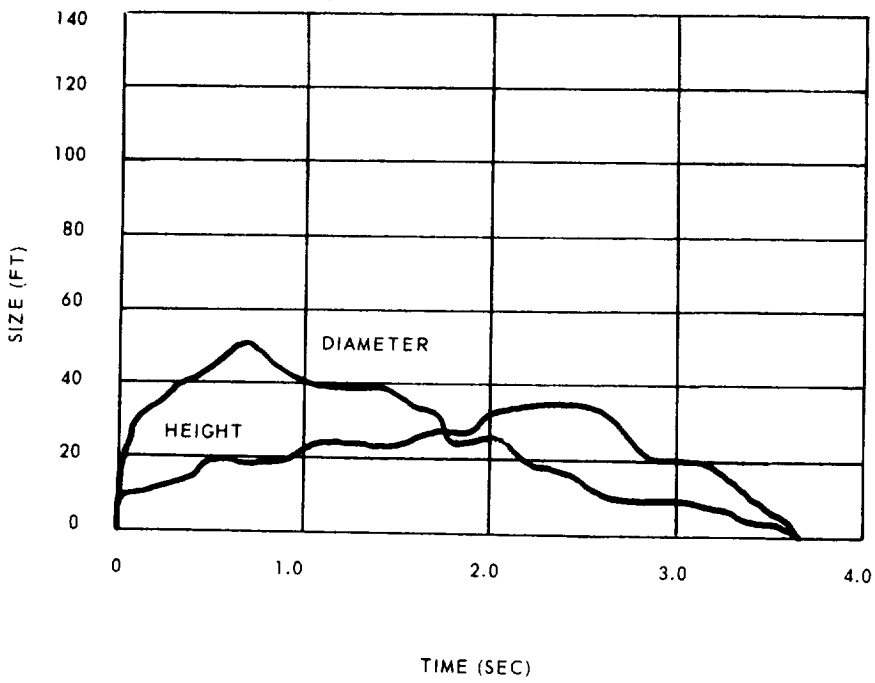

Test No. 7

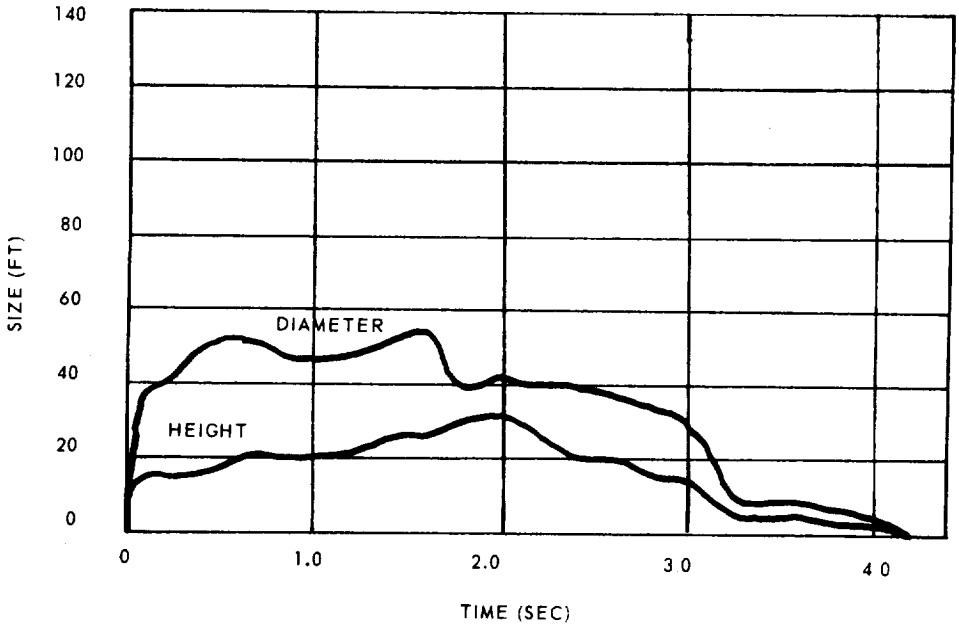

Test No. 8

Figure 17. Fireball History - N_2O_4/A-50 with Fall-Back Tankage.

Figure 18. N_2O_4/A-50 Fireball - Fall-Back Tankage.

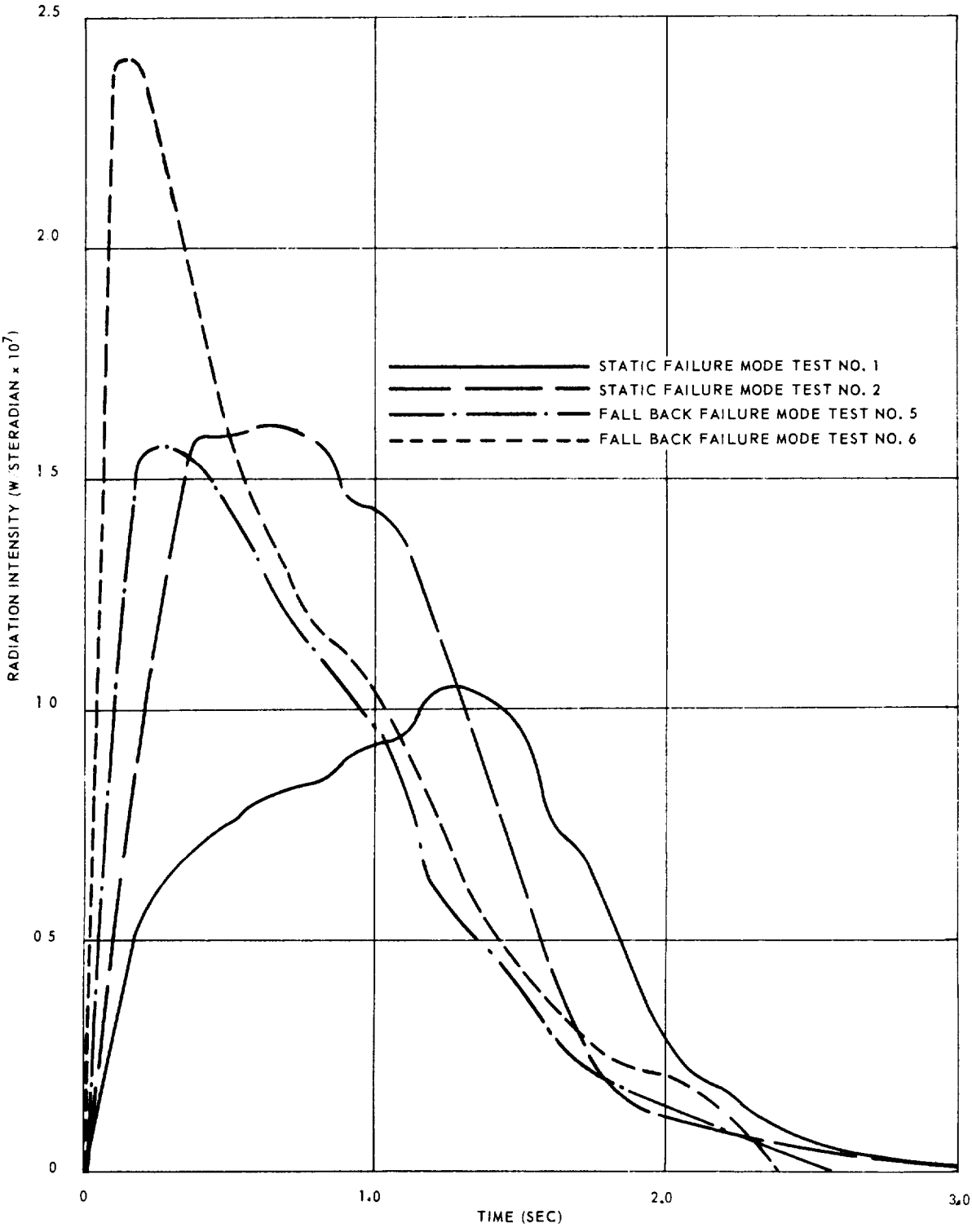

Figure 19. LOX/RP-1 Radiation Intensity.

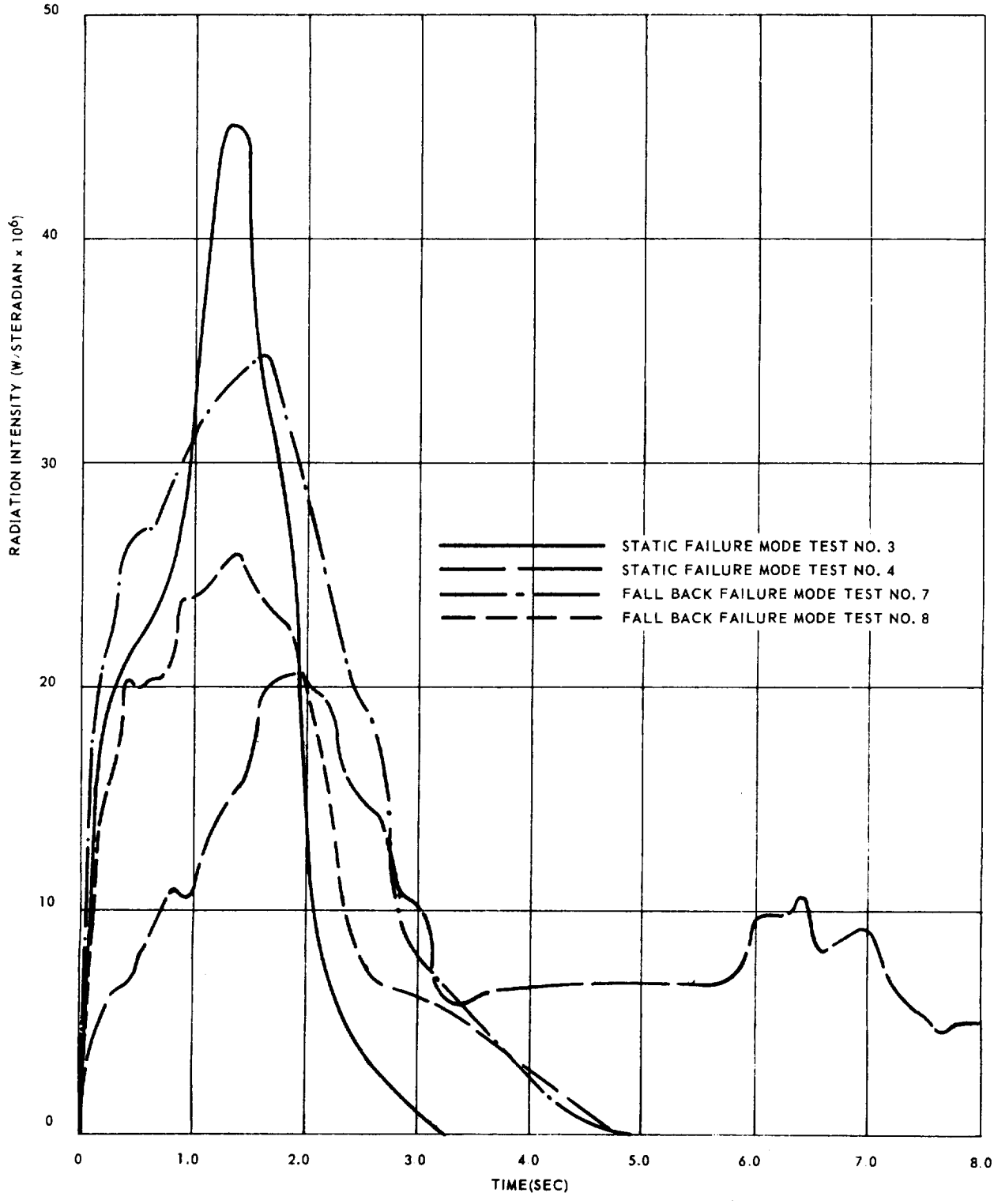

Figure 20. N_2O_4/A-50 Radiation Intensity.

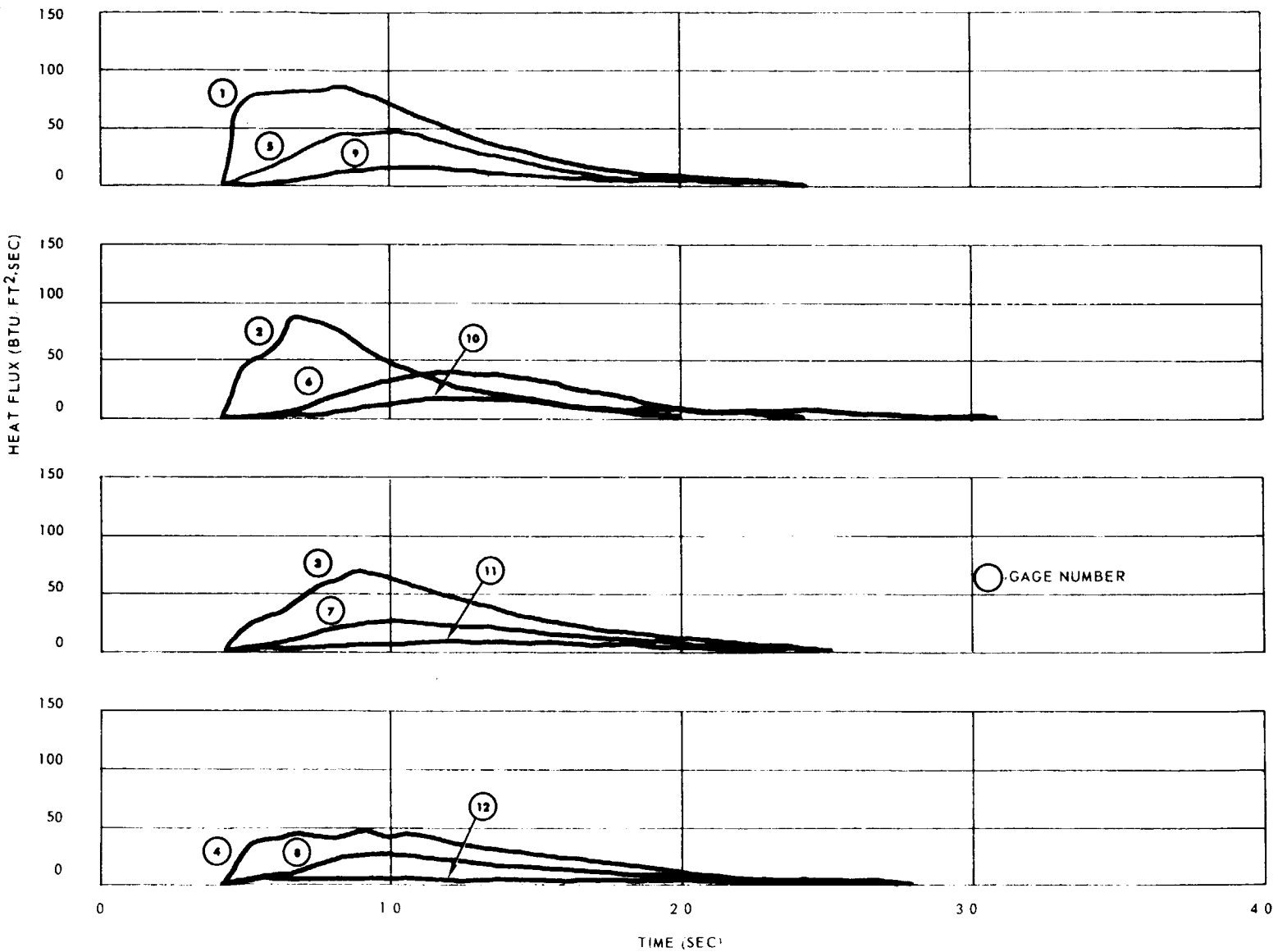

Figure 21. Heat Flux Record - Cryogenic Static Failure Mode Test.

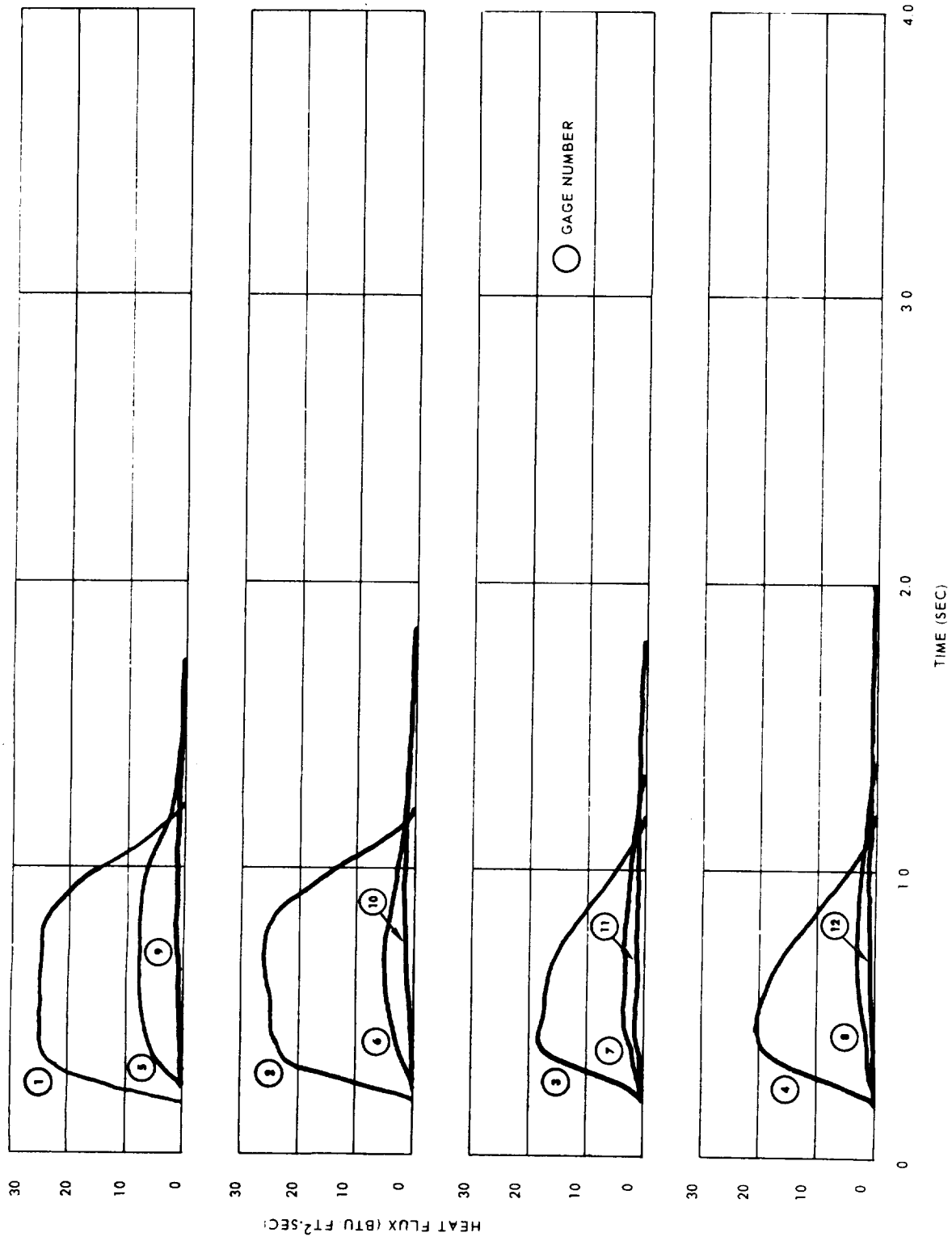

Figure 22. Heat Flux Record - Hypergolic Static Failure Mode Test.

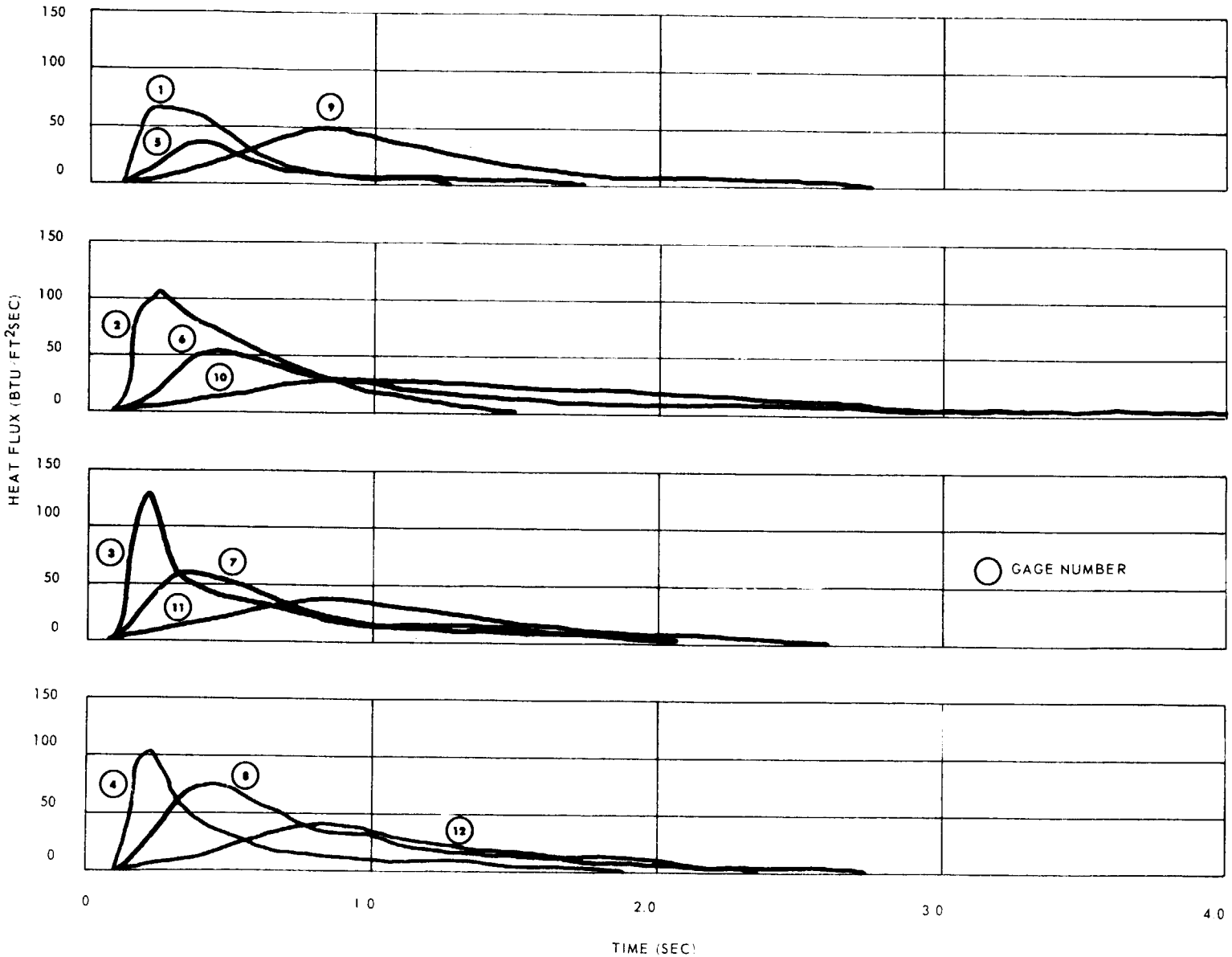

Figure 23. Heat Flux Record - Cryogenic Fall-Back Failure Mode Test.

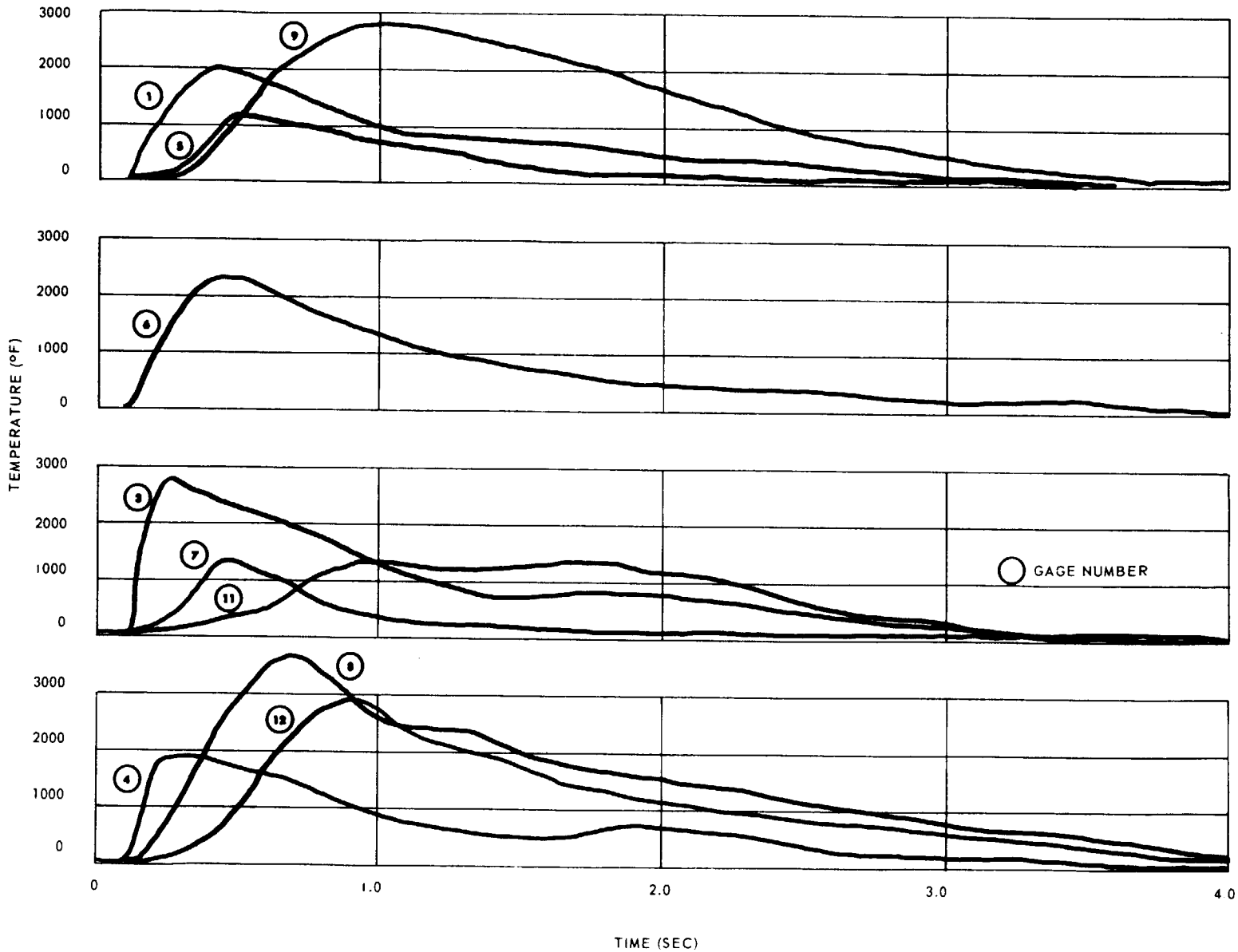

Figure 24. Temperature Record - Cryogenic Fall-Back Failure Mode Test.

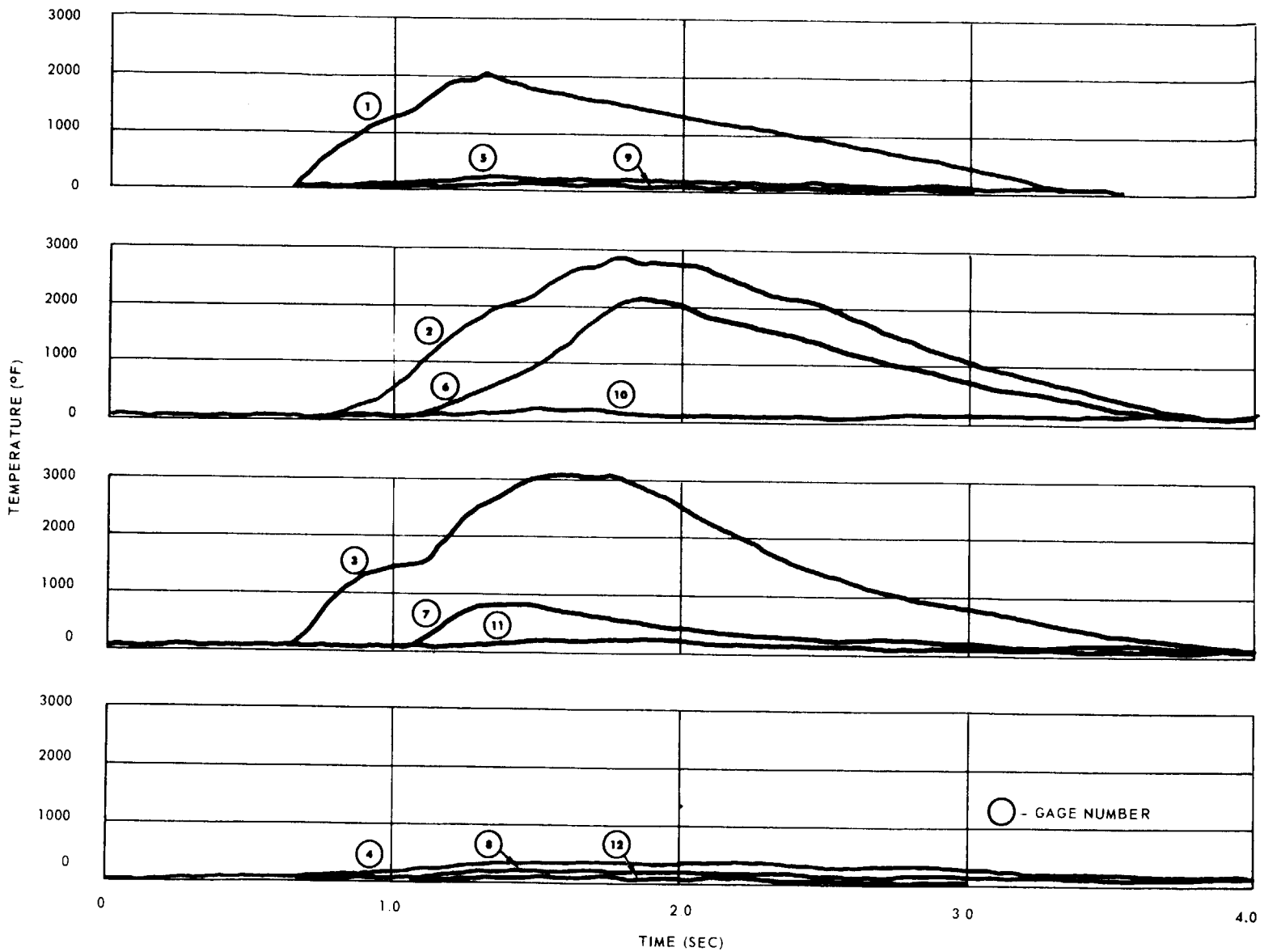

Figure 25. Temperature Record - Hypergolic Fall-Back Failure Mode Test.

BLACK AND WHITE PHOTOGRAPH

Figure 26. Remains of a Static Failure Mode Hypergolic Test.

Figure 27. Remains of a Static Failure Mode Cryogenic Test.

Figure 28. Remains of a Fall-Back Failure Mode Hypergolic Test.